
Book Section:
Tsavdaridis, KD orcid.org/0000-0001-8349-3979 (2014) Seismic analysis of steel–concrete composite buildings: numerical modeling. In: Beer, M, Kougioumtzoglou, IA, Patelli, E and Siu-Kui Au, I, (eds.) Encyclopedia of Earthquake Engineering. Springer-Verlag Berlin Heidelberg , pp. 1-36. ISBN 978-3-642-36197-5

https://doi.org/10.1007/978-3-642-36197-5_125-1

SEISMIC ANALYSIS OF STEEL-CONCRETE COMPOSITE BUILDINGS: NUMERICAL MODELING

by
Konstantinos Daniel Tsavdaridis

Table of contents:

Contents

Keywords: **seismic analysis, steel-concrete composite, numerical modeling, nonlinear, connections, T-stub components, panel zones, frames, concrete-encased steel sections, constitutive models, hysteretic rules, cyclic behavior, damping**

1. INTRODUCTION

1.1 Steel-concrete composite systems

Composite construction includes a wide range of structural systems, eg. framed structures employing all steel-concrete composite (SCC) members and components (eg. composite beam-to-columns and connections) and sub-assemblages of steel and/or reinforced concrete (RC) elements. Such components and elements are employed to optimize the resistance and deformation capacity (Uchida and Tohki 1997). SCC structures have been used extensively in recent years because of benefits in combining the two construction materials. SCC structures are also known for their excellent earthquake performance owing to their high strength, high ductility and large energy absorption. Their good structural damping properties arising from the friction between the steel-concrete interfaces make them an even more attractive alternative for seismic-resistance.

Consequent effects of combining the two materials are the enhanced lateral strength and stiffness of the frame, with apparent effects the alteration of the structural natural period of vibration, and the complex local behavior of beam-to-column connections. Furthermore, SCC beams subjected to lateral loading show complex behavior due to several factors, including the slip between the concrete slab and the steel beam, the variation of longitudinal stress across the width of the slab, and the overall configuration of the numerous different types of models while the steel and concrete parts can be subjected to different actions in every case. For the above reasons, the calculation of the seismic response of composite structures is not a straightforward task due to the interaction of local and global effects, and hence the unexpected failure modes that might incur. Consequently, it is very important for the analysis of such structures to account for the local interactions (eg. interface behavior between steel and concrete) as well as the local behavior of structural systems (eg. beam-to-column and base-to-column response). All these factors make the analysis of SCC structures and their individual components an intriguing but challenging task.

Although experimental procedures can be performed in order to enhance the understanding of the behavior of SCC structures under earthquake loading, they are typically expensive, time-consuming and do not cover a broad range of SCC structures and elements. As a result, numerical modeling procedures have been developed and tested in order to facilitate the analysis of such structures.

Most finite element (FE) packages (eg. ANSYS, ABAQUS, ADINA, DIANA, LS-DYNA, MIDAS FEA, etc.) rely on the use of constitutive models which emphasize on the description of post-peak material characteristics such as strain hardening and softening, tension stiffening, shear-retention ability, etc. (Cotsovos and Kotsovos 2011). The derivation of such constitutive models has been based on a variety of theories and their combination. However, the application of FE packages in practical structural analysis has shown that the constitutive relationships are case-study dependent, since the solutions obtained are realistic only for particular problems. Therefore, the applicability of packages to a different set of problems requires modifications of the constitutive relationships. This is entirely dependent on the interpretation of the observed material behavior as well as the use of the experimental data to validate the constitutive relationships.

To this end, the aim of the present chapter is to provide an indication of the concepts which are widely used for modeling the steel-concrete composite behavior and to develop numerical guidelines for the nonlinear analysis of such structures and their components, considering the seismic actions under earthquake events. The numerical analyses presented herein, model the behavior of SCC structures/components using macro-models (i.e. the use of line elements and spring connections) rather than micro-models (continuum FE models) due to their simplicity and accuracy in nonlinear analysis. Different aspects of modeling including the geometry, material nonlinearity (through the constitutive models adopted), hysteretic behavior and geometrical nonlinearity, as well as other parameters important for seismic analysis are also presented in this chapter.

1.2 Chapter Synthesis

The modeling of SCC elements and frames is based on three approaches. The first one is the simplified modeling approach presented in this chapter, engaging the use of springs and line elements for the elementary simulation of the behavior of each component to the entire frame assembly. The scope is to initiate numerical guidelines based on the simplified approach, and to present modeling examples of SCC cross-sections, beams, beam-to-column connections as well as the holistic approaches modeling a frame. The breakdown of this chapter is given in **Chart 1**.

Based on the bottom-up approach (i.e. combining different structural components starting from the most fundamental of a system and giving rise to grander systems),

the engineer will gain a decent understanding on the parameters to be considered during the computational modeling procedure. Modeling of these structural components will enable the computation of their response to different load histories, and moreover will enable the engineer to carry out the state determination of a member from a frame assembly.

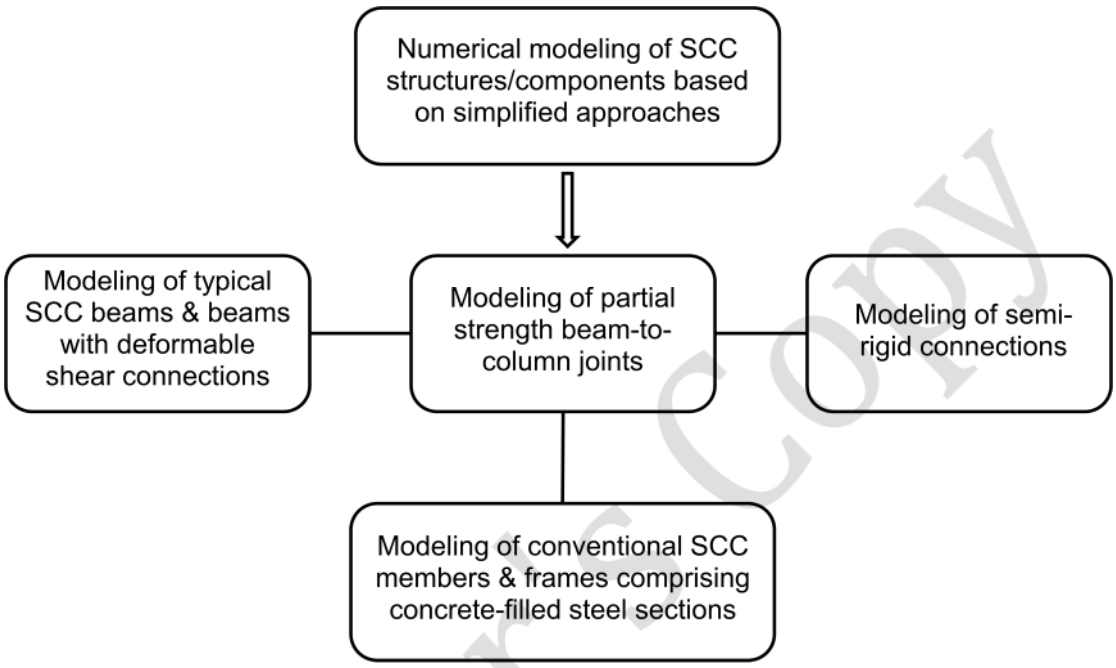

Chart 1: Structure of the chapter

1.3 Requirements for collapse analysis of composite structures

Numerical modeling procedures should aim to address a number of issues regarding the local, intermediate and global level of SCC structural design. On the *local* level, aspects such as the cyclic behavior of the steel and the concrete members (including the softening and hardening of the material), the local buckling of steel flanges, the load carrying capacity, the curvature ductility of the components as well as the effects of confinement should be carefully studied. On the *intermediate* level, the ductility of the member in terms of rotation/displacement should be established. Additionally, second order effects (P-Δ) on forces and deformations should be taken into account through the provisions for large displacement analysis. Modeling the beam-to-column connection is also essential when the fully-rigid assumption is not suitable. On the *global* level, the overall ductility and strength of the structure should be established through force-displacement relations. The progressive yielding and the hinge formation at the structural frame should also be established through

moment-rotation relationships. The complete list of requirements for the collapse analysis and the modeling of SCC structures subjected to earthquake actions is presented below:

- Stress-strain relationships for the steel material including strain hardening and softening.
- Provision for the effects of local buckling in the steel section.
- Stress-strain relationships for the concrete material including cycling loading regimes and the effect of the confinement on the peak stress and corresponding strain.
- Explicit representation of the slip boundary conditions of the shear connection both at local and global levels.
- Provision for second order effects on forces and deformations.
- Effective beam-to-column connection models, including panel distortion.
- Iterative and advanced dynamic analysis techniques for analyzing the structural response near collapse state.

2. MODELING OF STEEL-CONCRETE COMPOSITE SCC BEAMS

A variety of different models have been developed by researchers in order to capture the behavior of steel-concrete composite beams, based on either concentrated or distributed plasticity. In concentrated plasticity models, all the inelasticity is concentrated at the ends of the member; therefore it deals with material nonlinearity in an approximate but efficient manner. On the contrary, distributed models, model the inelastic behavior along the length of the member. This approach is more accurate but at the same time is more computationally demanding. Most of the formulations for both approaches are rather complex and not amenable to generic and routine application in structural engineering design.

The present sub-chapter presents a simplified (new) modeling approach based on the work of Zhao et al. 2012 for the nonlinear analysis of SCC beams and composite frames with deformable shear connections (based on the distributed plasticity approach) using line elements to simulate the structural beam and column members, layered fiber section to simulate the reinforced concrete slabs, and nonlinear spring elements for the simulation of the interface between the structural steel beams and the reinforced concrete slab. Vertical interactions between the slab and steel beams

are not expected to be significant, therefore are not accounted into the analysis. The geometry of the model, along with a simple set of details is outlined below. The assembled model is shown in **Figure 1**.

2.1 Model Geometry of a typical SCC beam

To model the geometry of the macro-model for a typical SCC beam, the following assemblies should be utilized:

1. Four-node layered shell elements representing the concrete slab. Reinforcement layers comprising steel material properties should be used to simulate the steel reinforcement located at the top and bottom of the concrete slab.
2. Two-node fiber beam-to-column elements for modeling the steel beam. The reference surface of the slab will be located at the centroid of the steel beam cross section.
3. Dummy nodes at the same locations as the beam-to-column element nodes simulating the connection between the nodes of the steel beam and the shell elements.
4. Rigid beam elements connecting the dummy nodes and the corresponding ones of the shell elements, located on the same x- and z- coordinates.
5. Discrete spring elements with only translation in the z-direction connecting both the dummy nodes and the beam-to-column element nodes in order to control the interface shear-slip surface along the length of the beam.

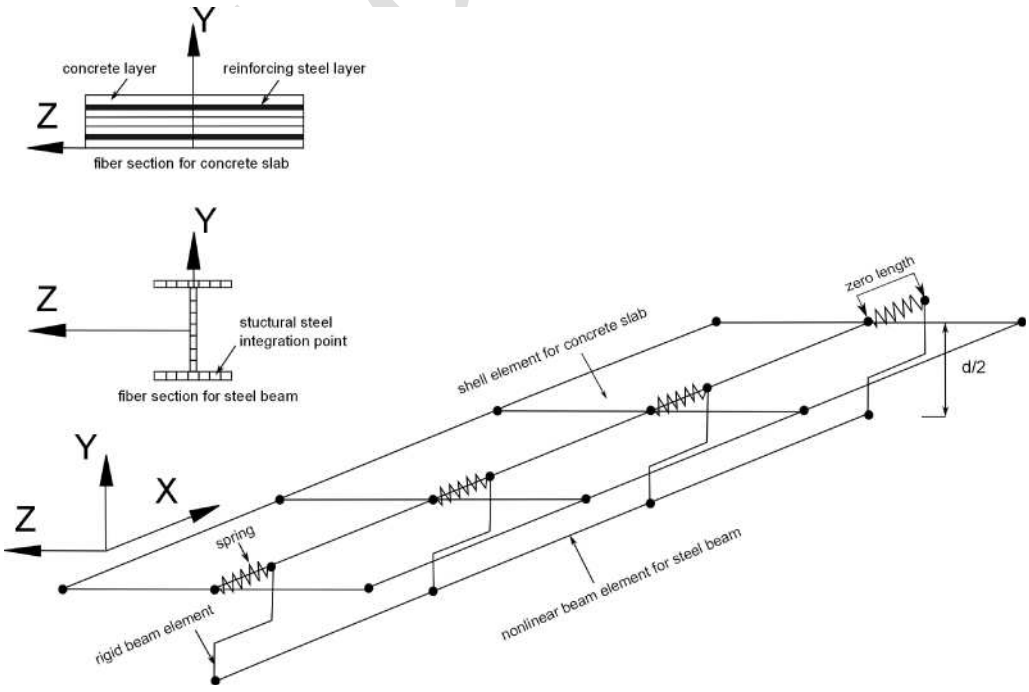

Fig. 1: Assembled macromodel representing a typical steel-concrete composite beam

2.2 Model Geometry of beam with deformable shear connection

Modeling of two-dimensional beams with deformable shear connection is based on the Newmark et al. 1951 model, in which (i) the Euler-Bernoulli beam theory applies to both components of the SCC beam and (ii) the deformable shear connection is represented by an interface model with distributed bond allowing interlayer slip as well as enforcing contact between the steel and concrete components.

A local coordinate system should be established to enhance the understanding of kinematics of Newmark's model. With reference to **Figure 2**, Z axis is parallel to the beam axis and the vertical plane YZ is the plane of geometrical and material symmetry of the cross section. Loads are also assumed symmetric with respect to the YZ plane. The displacement field u of a material point of the beam is given by:

$$u(y,z) = v(z)j + \left[w_a + (y_a - y)v'(z)\right]k \qquad \text{on } A_a \text{ (a =1, 2)} \qquad (1)$$

where w_a is the axial displacement of the reference point of domain A_a, the ordinate of which is y_a (a=1: concrete slab, a=2: steel beam); v is the vertical displacement of the cross section; and j and k denote the unit vectors along the Y and Z axes, respectively. It is observed that the transverse displacements and rotations of the slab and of the steel beam are equal due to the enforced contact between the two components. The only non-zero strain components are the axial strain ε_{za} and the interface slip δ.

$$\varepsilon_{za}(y,z) = w_a'(z) + (y_a - y)v''(z) \qquad \text{on } A_a \text{ (a =1, 2)} \qquad (2)$$

$$\delta(z) = w_2(z) - w_1(z) + hv'(z) \qquad (3)$$

Where: $h = y_2 - y_1$ is the distance between the reference points (G_1 and G_2 in **Figure 2**) of the two components. At the locations of the longitudinal reinforcement, Equation (2) also provides the strain in the reinforcement, due to the assumption of perfect bond between the steel and the concrete.

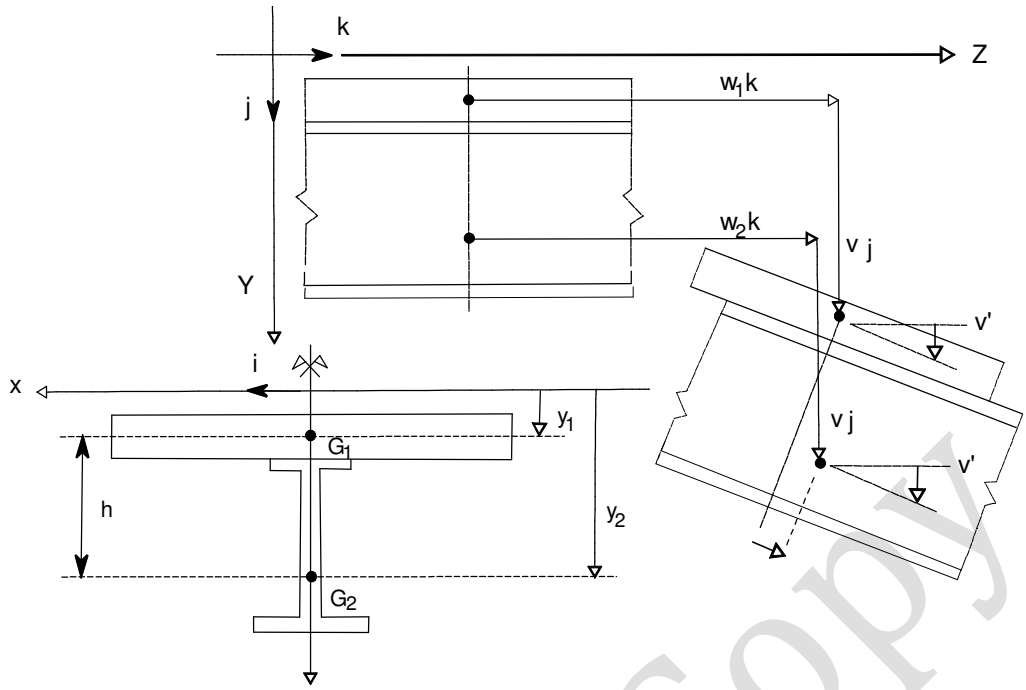

Fig. 2: Kinematics of two-dimensional composite beam model and reference system

2.2.1 FE formulations

A simple two-dimensional 10 degree-of-freedom (DOFs) SCC frame element with deformable shear connection is presented herein. With reference to **Figure 3**, 8 of the 10DOFs are external (4DOFs per end node) allowing for the axial displacement, the transverse displacement and the rotation of the steel beam and 1DOF for the axial displacement of the concrete slab. The remaining internal 2DOFs allow for axial displacement of the steel beam and the concrete slab (**Figure 3b**).

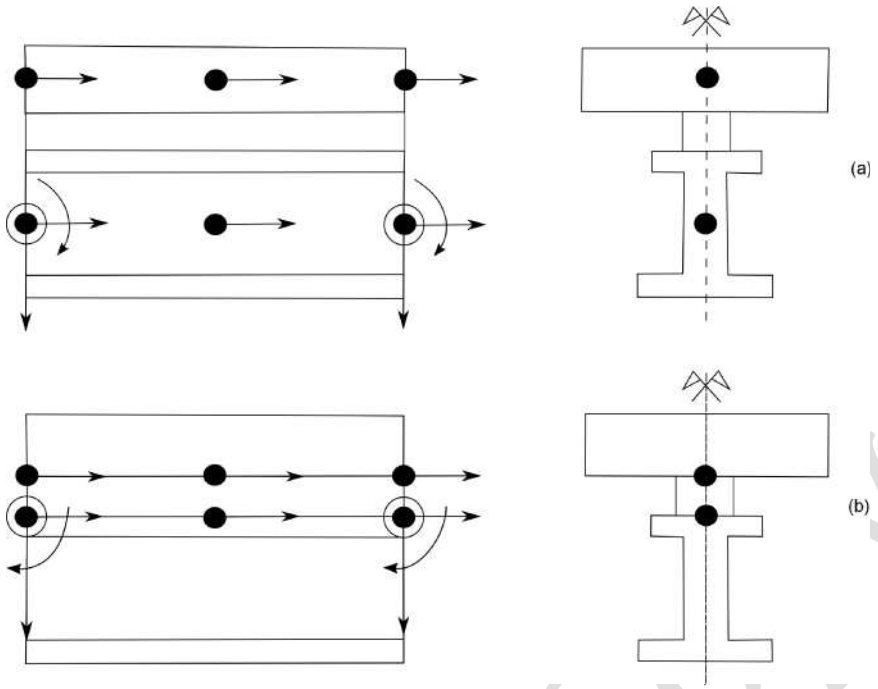

Fig. 3: 10DOF SCC beam element used a) references defined at the beam and slab centroids, b) references defined at the slab-beam interface

2.2.2 Modeling of inertia and damping properties

Modeling the inertia properties of the frame elements can be achieved using lumped masses at the DOFs of the external nodes. Consequently the inertia properties of the FE model are independent of the type of finite elements employed (i.e. the structure's mass matrix can be obtained using force, displacement or mixed-based formulation frame elements).

Even though the friction between steel beams and concrete slabs in SCC frames may be a strong source of structural damping, quantitative information about this energy dissipating mechanism usually referred to as structural damping is limited owing to the partial availability of experimental dynamic data. Consequently, the well-known and widely used Rayleigh damping model can be used by the practicing engineer. In this model, the damping matrix can be obtained using the classical Rayleigh damping relationship (Equation (4)) where the damping matrix is proportional to the mass matrix and the initial stiffness matrix.

$$[C] = \mu[M] + \lambda[K] \tag{4}$$

Where:

μ = mass proportional Rayleigh damping coefficient

λ = stiffness proportional Rayleigh damping coefficient

M = system structural mass matrix

K = system structural stiffness matrix

Note: The proposed model presented in the above sections considers only rigid beam-to-column connections. Nevertheless, semi-rigid connections can be considered in the same numerical procedure by introducing special joint elements with prescribed constitutive behavior.

2.3 Constitutive stress-strain relationships

For modeling purposes, the material properties (such as the Young's modulus, Poisson's ratio, elastic and plastic strength and strain hardening) can be obtained from the uni-axial stress-strain curves derived from coupon tests and then applied to the corresponding fibers across the composite cross section. In order to accurately simulate the behavior of SCC beams under earthquake conditions, robust material models capable of simulating the material nonlinearity as well as other damaging effects under dynamic or cyclic loading (i.e. softening/hardening) need to be employed. Several models have been developed to achieve the aforementioned scope, some of which are presented in the following sections.

2.3.1 Constitutive law for concrete parts (based on the Kent-Park model)

The proposed constitutive law modeling the concrete in monotonic compression for the cases of confined and unconfined concrete is the Kent-Park model as described in Park and Paulay 1975. As it is shown in **Figure 4**, the material follows a parabolic stress-strain curve up to a maximum stress equal to the cylinder's strength, after which it decays linearly with strain until the residual strength is reached. In tension, the model assumes a linear stress-strain behavior up until the tensile limit of the material is reached, and then the stiffness and strength decays with increasing strain (**Figure 5**).

The cyclic behavior of the concrete can be described by the Blakeley-Park model also presented in Park and Paulay 1975. The stress strain response lies within the Kent-Park envelope; however the effect of concrete confinement is not taken into account. The model assumes that unloading and reloading takes place along a line without energy dissipation or stiffness deterioration for strains smaller or equal to the strain corresponding to peak stress ($\varepsilon<\varepsilon_c$). Beyond this point, the stiffness

deterioration is taken into account through the introduction of reduction factors, given by Blakeley and Park. Along the first unloading branch, the stress is reduced approximately 50% without any reduction in strain. The reloading branch with slope equal to $f_c E$ extends back to the envelope (**Figure 5**).

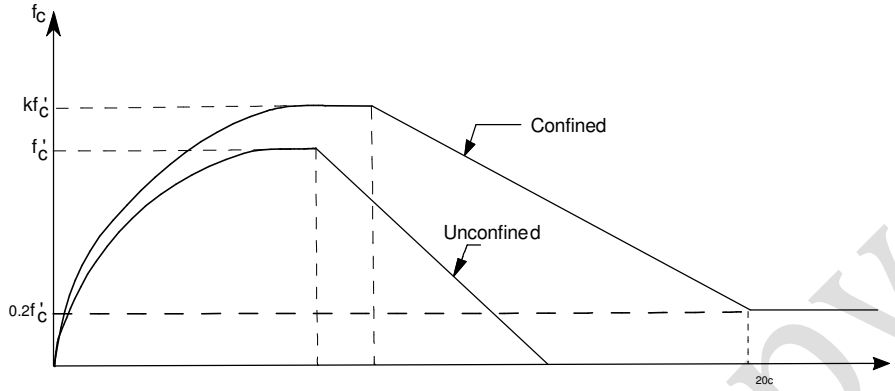

Fig. 4: Monotonic stress-strain Kent and Park model for unconfined and confined concrete

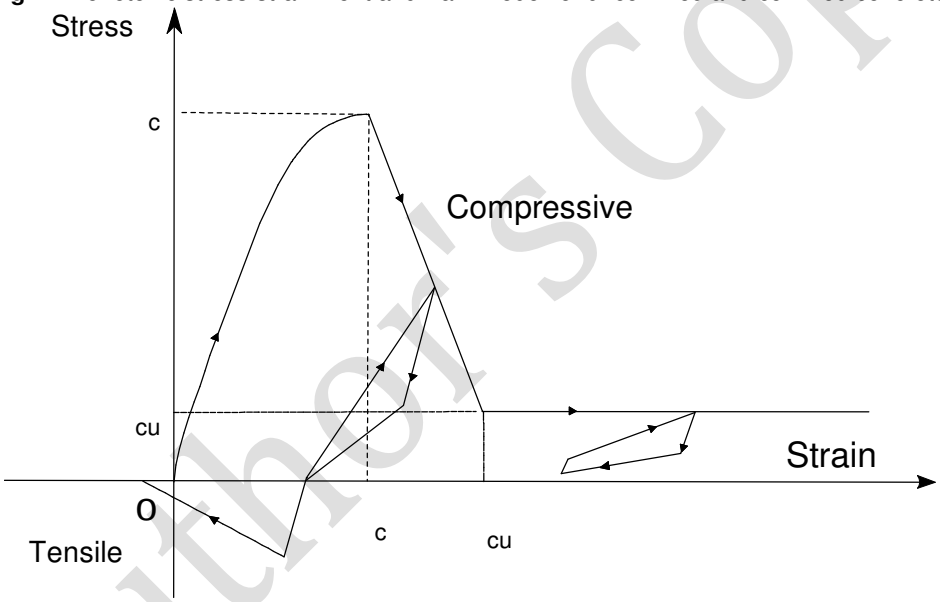

Fig. 5: Cyclic stress-strain Blakeley-Park model for concrete

2.3.2 Constitutive law for concrete (based on the Popovics-Saenz law)

The constitutive law for concrete is a uni-axial cyclic law with monotonic envelope defined by the Popovics-Saenz law (Balan et al.1997). Linear unloading-reloading branches with progressively degrading stiffness characterize the cyclic behavior of the material. The response of concrete under cyclic loading is shown in **Figure 6**. According to the same figure, after each unloading-reloading, the monotonic envelope is reached again when the absolute value of the largest compressive strain attained so far is surpassed. The tensile behavior of concrete is characterized by the

same loading-unloading-reloading rules with the same initial stiffness and appropriate values for the other parameters.

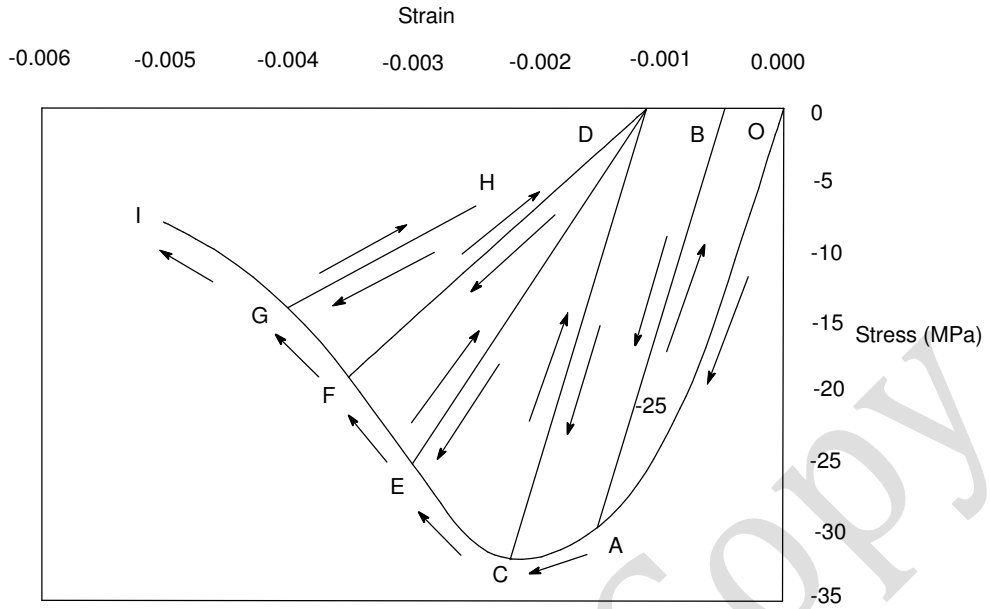

Fig. 6: Hysteretic concrete material model under compression

2.3.3 Constitutive law for steel

Figure 7a and **7b** describe the elasto-plastic response of the steel under monotonic and cyclic loading respectively. For monotonic loading, the characteristic yield plateau in the stress-strain model followed by a region of increased strength owing to strain hardening of the material. The unloading from the yielded condition is elastic; thereafter, the Bauschinger effect can be represented by a Ramberg–Osgood relationship (Equation (5)) until the yield stress is reached. This model uses a single non-linear equation to characterize the observed curvi-linear response of steel subjected to monotonic loading.

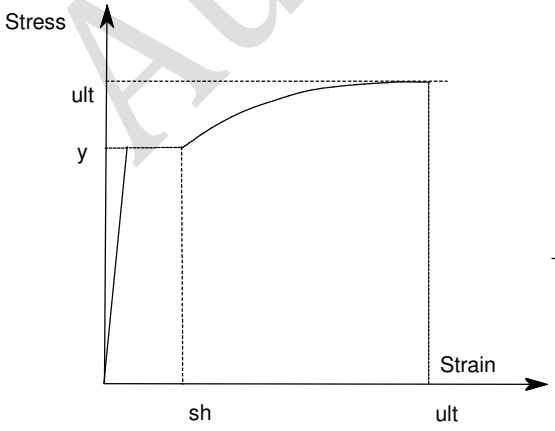

Fig. 7a: Stress-strain model under monotonic loading

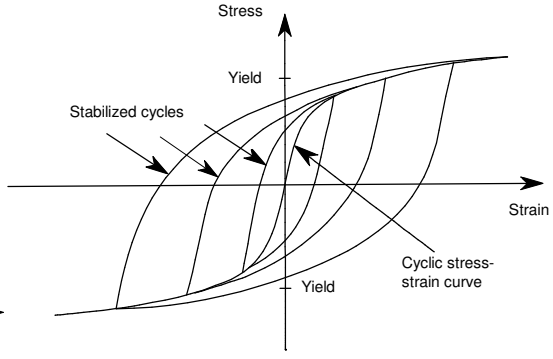

Fig. 7b: Steady state cyclic response of mild steel

$$\varepsilon = \frac{\sigma}{E} + K\left(\frac{\sigma}{E}\right)^{\eta} \qquad (5)$$

Where:

$\frac{\sigma}{E}$ = equal to the elastic part of the strain

$K(\frac{\sigma}{E})^{\eta}$ = accounts for the plastic part of the strain

K and η = parameters that describe the hardening behavior of the material

When the steel material is subjected to constant strain ampliutude under cyclic loading, it exhibits a response which converges to a stabilized saturation loop which depends only on the cycling amplitude (**Figure 7b**). As it is shown in **Figure 8**, the response of the steel material under constant strain amplitude cycles, is described by strain hardening for large amplitudes and strain softening for small amplitudes. For the accurate simulation of the steel material response under an arbitrary load, the constitutive model needs to account for all, the monotonic response, the steady-state cyclic behavior as well as the transient behavior involving softening and hardening. This can be achieved using an efficient simplistic computationally bi-linear model.

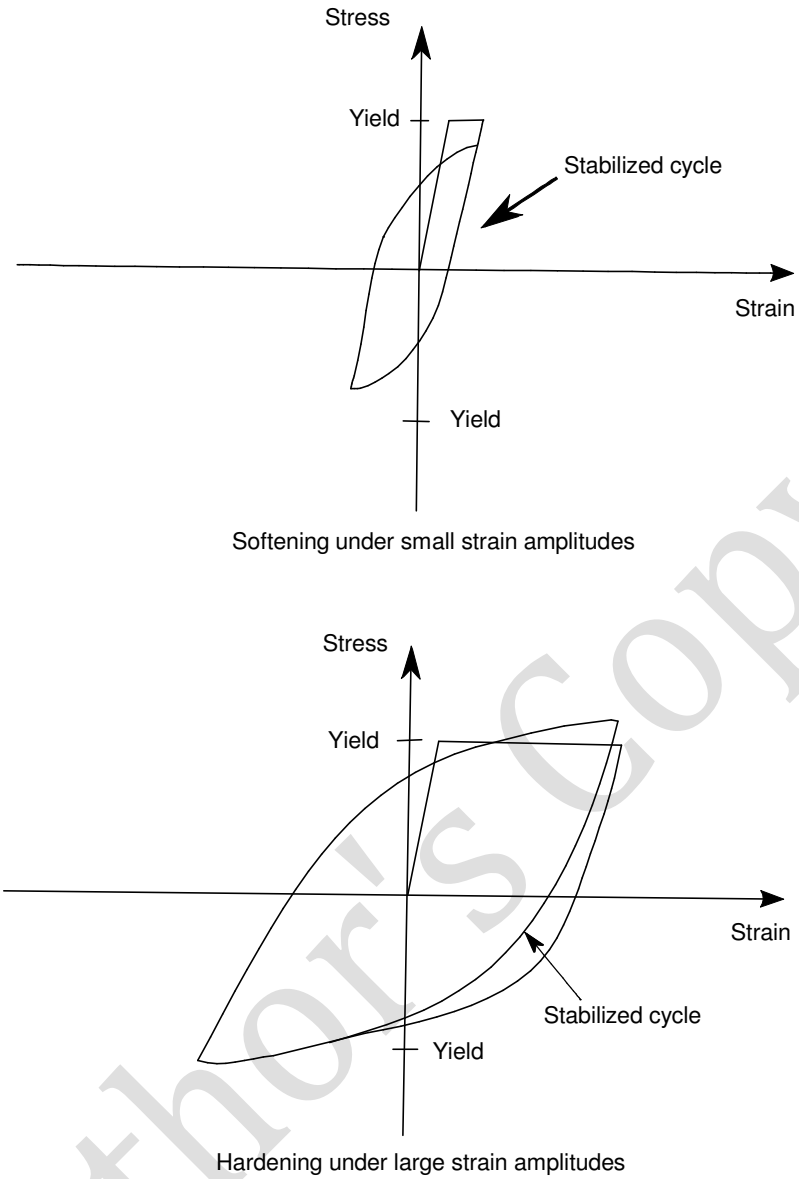

Fig. 8: Cyclic response of steel under constant strain amplitude cycles

2.2.2.1 Bi-linear stress-strain steel model

In this bi-linear model, the elastic range remains constant throughout the various loading stages. The kinematic hardening rule for the yield surface is assumed to be a linear function of the increment of plastic strain (**Figure 9**). The calculation of the current stress state is expressed mathematically using Equations (6) to (8) and it is presented graphically in **Figure 10**:

$$\left.\begin{aligned}\alpha &= \alpha^0 \\ \sigma &= \sigma^0 + E(\varepsilon - \varepsilon^0)\end{aligned}\right\} \quad \text{If } \left(\frac{\alpha - \sigma_y - \sigma^0}{E}\right) \leq (\varepsilon - \varepsilon^0) \leq \left(\frac{\alpha^0 + \sigma_y - \sigma^0}{E}\right) \qquad (6)$$

$$\left.\begin{aligned}\alpha &= \alpha^0 + \mu E\left(\varepsilon - \varepsilon^0 - \frac{\alpha^0+\sigma_y-\sigma^0}{E}\right)\\ \sigma &= \alpha + \sigma_\gamma\end{aligned}\right\} \quad \text{If} \quad (\varepsilon - \varepsilon^0) > \left(\frac{\alpha^0+\sigma_y-\sigma^0}{E}\right) \qquad (7)$$

$$\left.\begin{aligned}\alpha &= \alpha^0 + \mu E\left(\varepsilon - \varepsilon^0 - \frac{\alpha^0-\sigma_y-\sigma^0}{E}\right)\\ \sigma &= \alpha - \sigma_\gamma\end{aligned}\right\} \quad \text{If} \quad (\varepsilon - \varepsilon^0) < \left(\frac{\alpha^0-\sigma_y-\sigma^0}{E}\right) \qquad (8)$$

Where according to **Figure 9** and **10**:

E = Young's modulus

μ = strain hardening parameter

σ_γ = initial yield surface

ε = current strain

σ = current stress

α = current centre of elastic range

Subscript "0" denotes values at the start of an increment

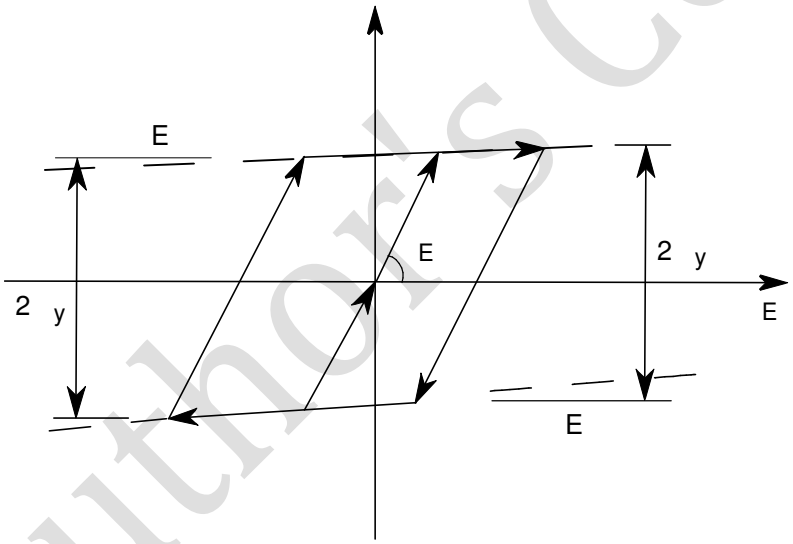

Loading and unloading paths of bi-linear of bi-linear kinematic model

Fig. 9: Loading and unloading paths of bi-linear kinematic model

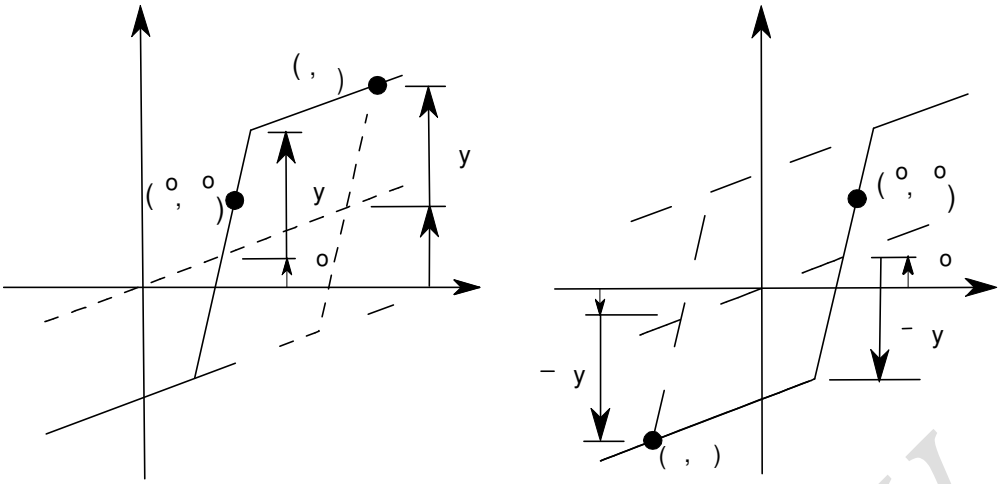

Positive strain increment

Negative strain increment

Fig. 10: Stress determination with the bi-linear kinematic model

2.2.3 Constitutive law for steel (based on the Menegotto-Pinto model)

The constitutive law describing the behavior of the steel material is the uni-axial Menegotto-Pinto model (1973). This computationally efficient non-linear law is capable to model both kinematic and isotropic hardening as well as the Bauschinger effect, allowing for accurate simulation and reproduction of experimental results. The response of the steel material is defined by the following non-linear equation:

$$\sigma = b\,\varepsilon + \frac{(1-b)\varepsilon}{(1+\varepsilon^{R})^{\frac{1}{R}}} \tag{9}$$

Where the effective strain and stress (ε, σ) are a function of the unload-reload interval, b is the ratio of the initial to final tangent stiffness and R defines the shape of the unloading-reloading curves. **Figure 11** presents a typical stress-strain response based on the Menegotto-Pinto model. The model assumes a symmetric response for loading in compression and tension.

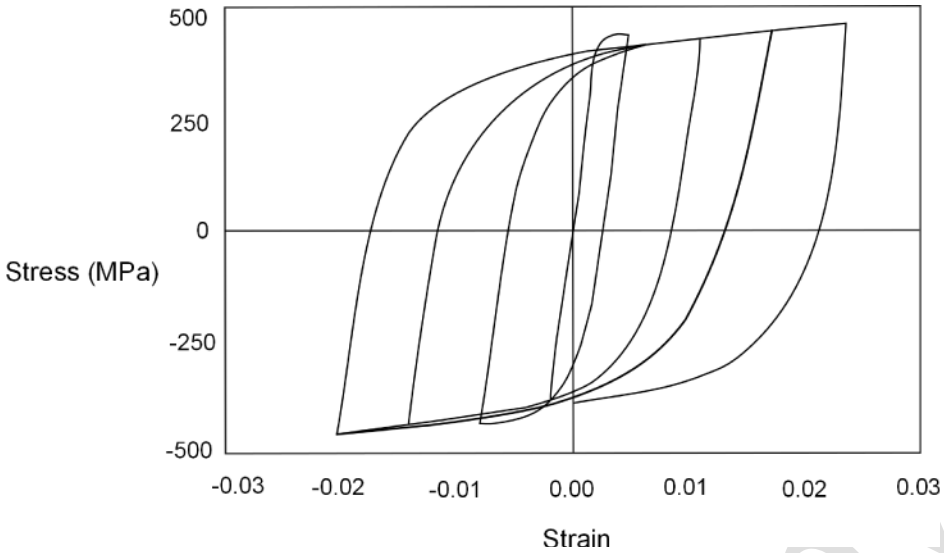

Fig. 11: Menegotto-Pinto material constitutive model for structural steel; typical cyclic stress-strain response

2.4 Interaction of material surfaces: evaluation of spring properties

The degree of composite action and interaction between the steel beam and the concrete slab is a fundamental mechanism that needs to be considered by the engineer during the modeling procedure of SCC beams and structural systems owing to the implications on the serviceability and ultimate limit states, the energy dissipation under cyclic loading, and the local stress distribution.

Two different modeling approaches can be used for the description of partial bond in SCC structural systems. The concentrated bond approach is based on the use of concentrated springs for the modeling of the connection. The springs are attached at the location of each connector, modeling either the action of the shear stud connectors between the steel and the concrete slab or the friction in concrete filled hollow sections and partially encased steel sections. The second approach is based on the distributed bond model, assumes a continuous bond stress and bond slip along the contact surface. For both approaches the uplift is typically neglected, therefore it is considered that the concrete slab and the steel beam have the same vertical displacement and curvature.

Shear-slip relationships are widely available providing information regarding the behavior of the connectors. **Figure 12a** presents a simplified bi-linear shear-slip relationship based on a widely used shear-slip model proposed by Ollgaard 1971. The Ollgaard model is described by the following exponential function (Equation (10))

representing an experimentally observed large reduction of stiffness with increasing slip.

$$\frac{N_v}{N_{vu}} = (1 - e^{-ns})^m \quad (10)$$

Where:

N_{vu}= connection (ultimate) strength

N_v = shear load

s = slip between two components of the composite beam (interface slip)

n , m = empirical parameters defining the shape of the curve calibrated from experimental data

In **Figure 12b**, the monotonic envelope is presented by the definition of an ultimate slip, S_{ult}. When ultimate slip, the shear force-slip behavior follows zero-stiffness with constant shear force N_v = +- τ_{fr}, where τ_{fr} is the residual shear force.

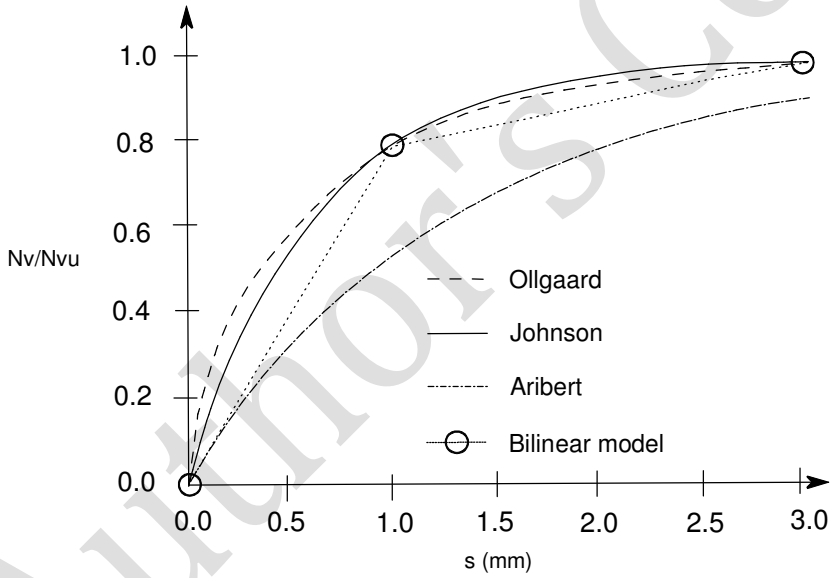

(a) Equivalent bi-linear model for shear-slip of each connecto r

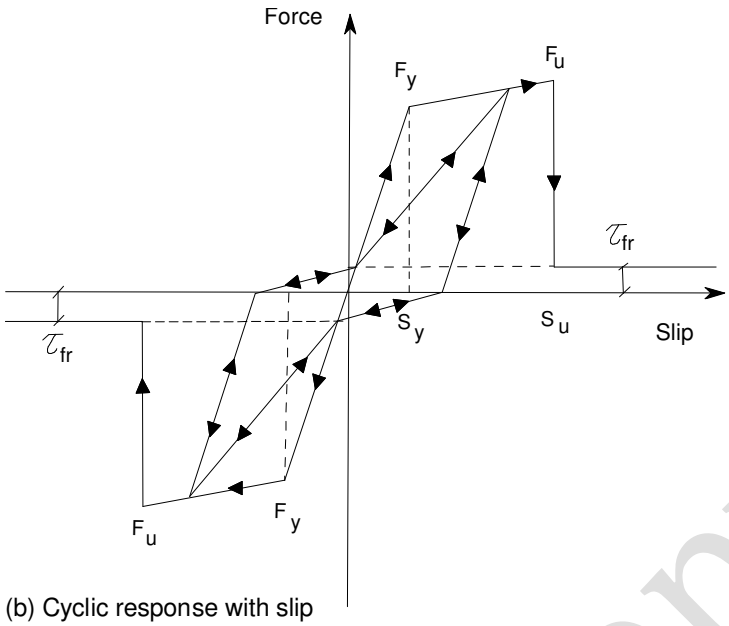

Fig. 12: Shear-slip relationships

3. MODELING OF STEEL CONCRETE COMPOSITE BEAM-TO-COLUMN PARTIAL STRENGTH SEMI-RIGID CONNECTIONS

Compared to traditional bare steel structures, SCC frames can achieve more effective beam-to-column connections through the contribution of the concrete slab in resisting bending moments under gravitational and lateral loads. Additionally, these structures comprising partial-strength partially restrained beam-to-column joints designed in such a way to exhibit ductile seismic response through the plastic deformation of their components can achieve the formation of a desirable beam hinging global frame mechanism, with large hysteretic energy dissipation capacity and reduced force demand on the columns.

This section of the chapter presents a simplified approach based on the work done by Braconi et al. (2007) for the non-linear analysis of a partial strength beam-to-column connection using a component model. The behavior of partial strength beam-to-column connections under the application of seismic load is described using non-linear spring elements as shown in **Figure 13**. With reference to the same figure, the elements comprising the model should account for the response of the:

1. Concrete in compression
2. Column web panel in shear
3. Upper T-stub in compression (+ Ve moment)

4. Lower T-stub in tension (+Ve moment)
5. Concrete slab in tension
6. The shear studs (+Ve moment)
7. Upper T-stub in tension (-Ve moment)
8. Upper T-stub in compression (-Ve moment)
9. Shear studs (-Ve moment)

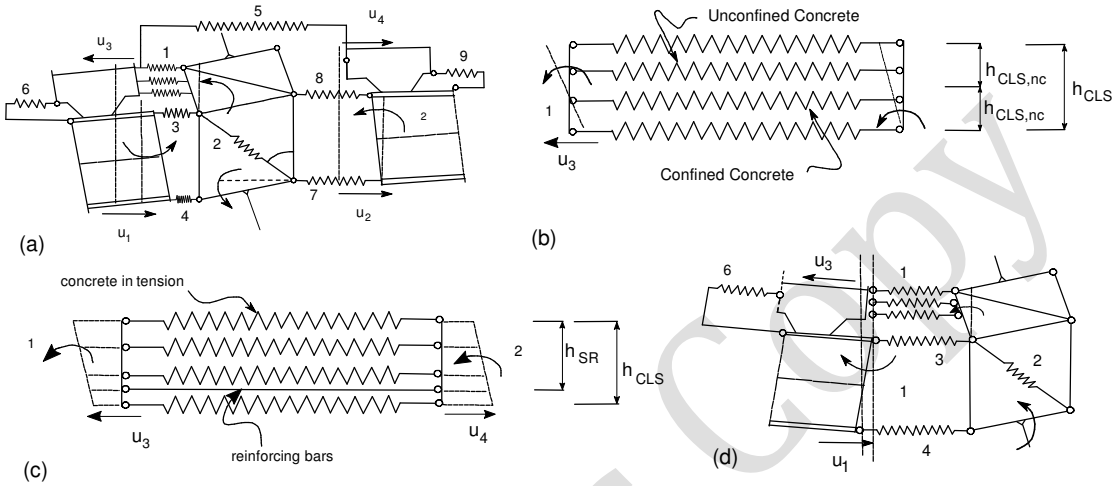

Fig. 13: Component model: a) overall joint model; b) kinematics of the concrete slab in compression (component 1); c) kinematics of the concrete slab in tension (component 5) and d) overall exterior joint model.

3.1 Kinematics

Equilibrium must be maintained between the force acting in the nine components and the internal and external forces. The response of the assembled model is therefore defined by a set of eight equations related to translational equilibrium between components in the same beam-to-column connection, equilibrium between the shear studs and the beam steel profile, rotational equilibrium between the internal forces in the beam-to-column connection and the bending moment of the beam framing in it as well as rotational and translation equilibrium acting on the column web panel. The set of eight equations can be then solved using a numerical procedure (i.e. Newton-Raphson) considering the story deformation (drift, δ) as such an external action in the format of imposed deformations.

On the basis of the small displacement theory, the local kinematics could be described using a total 7DOFs: the horizontal displacement of the bottom surface of the slab on both sides of the column: u_1 and u_2, the horizontal displacement of the top surface of the slab on both sides of the column: u_3 and u_4, the relative rotation of

the two beams with respect to the column faces: θ_1 and θ_2, and the column panel zone shear distortion: γ. The deformations, δ, of the 9 components comprising the model, are linked to the seven degrees of freedom through the following equations:

$$\delta_{1,i}^{nc} = -u_3 - \frac{\Delta_{nc}}{2} * (2i - 1)\tan(\theta_1) + \left[h_{cs} - \frac{\Delta_{nc}}{2}(2i - 1)\right]\tan(\gamma) \quad (11)$$

$$\delta_{1,i}^{c} = -u_3 - \left[\frac{\Delta_c}{2}(2i - 1) + h_{cls,nc}\right]\tan(\theta_1) + \left[h_{cls} - \frac{\Delta_c}{2}(2i - 1)\right]\tan(\gamma) \quad (12)$$

$$\delta_3 = -u_1 - (h_{cs} + \frac{t_{bf}}{2})\tan(\theta_1) \quad (13)$$

$$\delta_4 = -u_1 - (h_{cs} + h_b - \frac{t_{bf}}{2})\tan(\theta_1) \quad (14)$$

$$\delta_{5,i} = u_4 - [h_{cs} - \frac{\Delta_{ct}}{2}(2i - 1)]\tan(\theta_2) - u_1 - [\frac{\Delta_{ct}}{2}(2i - 1)]\tan(\theta_1) \quad (15)$$

$$\delta_{5,SR} = u_4 - (h_{cs} + h_b - \frac{t_{bf}}{2} - h_{SR})\tan(\theta_2) - u_1 - h_{SR}\tan(\theta_1) \quad (16)$$

$$\delta_6 = u_1 - u_3 \quad (17)$$

$$\delta_7 = u_2 \quad (18)$$

$$\delta_8 = u_2 - (h_b - t_{bf})\tan(\theta_2) \quad (19)$$

$$\delta_9 = u_2 - u_4 \quad (20)$$

In the above equations, h_b is the beam depth, h_{cs} is the overall slab thickness including the depth of the steel deck, but the model assumes that the interaction between the slab and the column only occurs over the slab thickness above the steel deck, h_{cls}, to represent actual test conditions. The parameter, t_{bf}, is the beam flange thickness. For components 1 and 5, the deformation varies among the series of n parallel springs used over the slab thickness. For the concrete in compression (Component 1), a distinction is also made between unconfined $(\delta_{1,i}^{nc})$ and confined $(\delta_{1,i}^{c})$ concrete fibers. Unconfined concrete condition is assumed above the slab reinforcing steel (of thickness $h_{cls,nc}$in **Figure 13b**), and therefore the parameters Δ_c and Δ_{nc} correspond to the thickness of each confined and unconfined concrete layers, respectively. Similarly, Δct is the thickness of the concrete layers in tension. **Figure 14** presents the deformation of the entire sub-assemblage. The story drift, δ, is obtained through Equation (21).

$$\delta = \gamma \cdot h_{SP} + \varphi \cdot h_{tot} + \delta_{el,column} \quad (21)$$

Where the first term represents the storey drift owing to the web panel over the height of the joint, h_{SP}, the second term corresponds to the rotation due to flexural deformations of the beam at beam mid-depth, and the final term corresponds to the elastic flexural deformation of the column. **Figure 14** shows the global kinematics of the model.

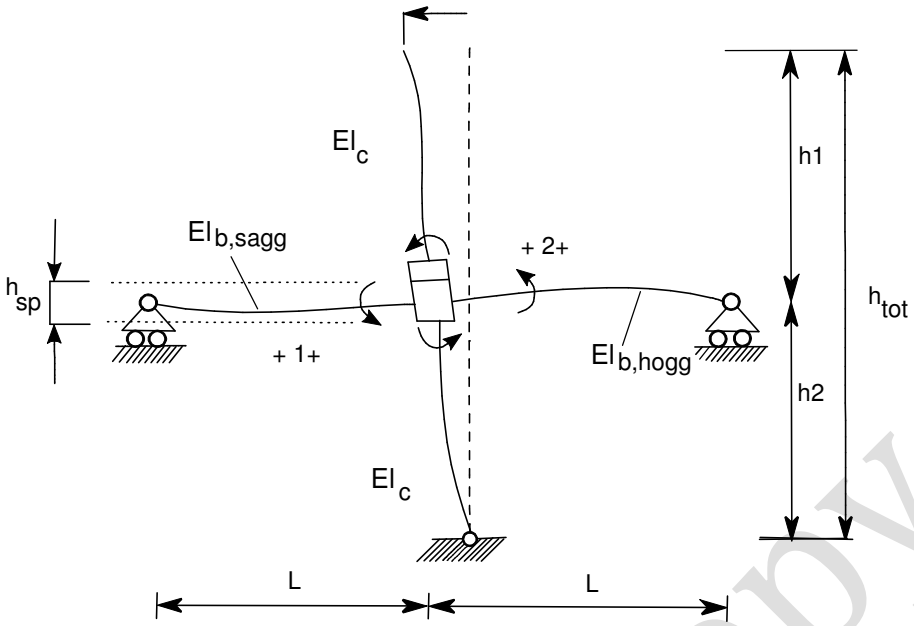

Fig. 14: Global kinematics of the sub-assemblage joint specimen

3.2 Component modeling

Necessary work preceding the assembling of a SCC connection model is the verification of each individual component model. In a semi-rigid SCC connection the major components to be considered are outlined below.

3.2.1 Concrete slab

The non-uniform stress distribution over the slab thickness is taken into account in the model with the use of fibers as shown in **Figures 13b and 13c** for the cases of compression and tension, respectively. Concrete slab in compression can be modeled using stress-strain relationships proposed in EC2 or any of the stress-strain relationships presented in sub-sections 2.3.1 and 2.3.2 for both unconfined (concrete above reinforcement level) and confined (concrete below reinforcement level) conditions. A typical example of the stress-strain relationship that can be used in analysis is presented in **Figure 15a** for both concrete conditions. In tension (**Figure 15b**), the behavior of concrete can be represented using a linear response until cracking, followed by a softening branch where the tensile resistance reduces exponentially as proposed by Stevens et al. 1991. Linear unloading- reloading branches can be adopted intersecting the deformation axis at a residual plastic deformation ε_{ct}^{pl} given by Equation (22) and also shown in **Figure 15b**:

$$\varepsilon_{ct}^{pl} = 146\,(\varepsilon_{ct}^{max})^2 + 0.523\,(\varepsilon_{ct}^{max}) \quad (22)$$

3.2.2 Steel reinforcement

Bi-linear stress-strain relationships as shown on **Figure 15c** can be adopted for representing the behavior of steel reinforcement.

3.2.3 Shear connectors

The slip between the concrete slab and the beam owing to the flexibility of the shear stud connectors can be modeled using force deformation relationships similar to those presented earlier in section 2.4 ('simulation of composite action'). The recommended force-deformation relationship for this particular model is the one proposed by Aribert and Lachal 2000 (which uses the guidelines of EC4 and EC8 for the calculation of the ultimate shear stud resistance) and it is presented in **Figure 15d** and Equation (23).

$$F = Q_u(1 - e^{(C_1(u_3 - u_4))^{C_2}} \quad (23)$$

Where:

Q_u = ultimate shear stud resistance calculated according to EC4 and EC8

C_1, C_2 =Coefficients suggested by Aribert and Al Bitar 2000 depending on the height of studs and type of steel profile.

3.2.4 Panel zone in shear

The behavior of the panel zone plays a significant role in determining the overall stiffness and capacity of the frame. In terms of seismic design, the panel zone can have a significant influence on the distribution of plasticity and energy dissipation on the overall performance of the structure. A multi-linear shear force to shear deformation response is retained for the web panel zone. The following equations describe this multi-linear relationship through the gradients of elastic, post-elastic and strain hardening stiffness as follow:

$$K_{el,wp} = G_S \frac{A_{vc}}{z} \quad (23)$$

$$K_{t,wp} = 1.04\, G_S \frac{b_{cf}\, t_{cf}^2}{z} \quad (24)$$

$$K_{s,wp} = \frac{G_S}{a_H} \frac{(h_c - t_{cf})t_{cw}}{z} \quad (25)$$

Where:

G_S = shear modulus of steel

A_{vc} = shear area of the column section

z = centerline vertical distance between the column stiffeners

b_{cf} = column flange width

t_{cf} = column flange thickness

h_c = column depth

t_{cw}= column web thickness

a_H = hardening coefficient related to the thickness of the column web panel and the column flanges

Using the elastic and post-elastic stiffness, shear forces in the panel zone can be obtained. The elastic stiffness, $K_{el,wp}$, is obtained from EC3 and is applicable until the shear force, V_{wp}, reaches the yield limit, $V_{el,w}$, which is also specified in EC3 (Equation (26)). The shear forces corresponding to the post-elastic branches, described by Krawinkler's model (Krawinkler 1978), in which the shear force is obtained through Equation (27) and (28). The three different branches of the shear force to deformation relationship are presented in **Figure 15e** (dashed line).

$$V_{el,wp} = \frac{0.9\, f_{y,cw}\, A_{vc}}{\sqrt{3}} \tag{26}$$

$$V_{t,wp} = \frac{0.9\, f_{y,cw}\, A_{vc}}{\sqrt{3}} + 1.04\, G_S \frac{b_{cf}\, t_{cf}^2}{z}\, 3\, \gamma_\gamma \tag{27}$$

$$V_{s,wp} = \frac{f_{u,cw}\, A_{vc}}{\sqrt{3}} + \frac{f_{u,cf}\, b_{cf}\, t_{cf}^2}{4z} \tag{28}$$

Where:

γ_γ = panel distortion at yield = $V_{el,wp}/K_{el,wp}$

$f_{u,cw}$, $f_{u,cf}$ = ultimate tensile stress for column web and flanges

3.2.4 T-stubs components

The geometry of the equivalent T-stub components can be determined using the effective width concept presented in EC3 for stiffened columns and end-plates. The force-to-deformation relationship of T-stub elements required for component modeling can be obtained from the model proposed by Piluso 2001 (dashed line) (**Figure 15f**).

3.3 Simplifications and assumptions

1. The difference in column web shear stiffness between the concrete encased and non-encased segments of the columns should be taken into account in

modeling through the assumption of infinite stiffness of the upper encased portion of the column and a flexible diagonal spring in the bare steel column web over the beam depth.

2. Bolt pretension effects need to be considered in modeling through modification of the stiffness of the equivalent T-stub springs in the elastic range.
3. There is an interaction between the connections on both column sides due to the continuity of the slab and the slab longitudinal steel reinforcement between the two beams. Hence, including the anchorage steel bars the negative moment capacity of one side is dependent on the concrete capacity of the opposite side, while essentially transferring the tensile forces acting from the reinforcing steel to the column. The modeling engineer can use more advanced modeling procedures (i.e. as proposed by Fabbrocino et al. 2002) when continuous SCC beams are considered for the assessment of the behavior of the connection capacity, in terms of global quantities such as the rotations and deflections as well as local quantities such as the slip and the curvature of members, the interaction forces, and the rebar strain.
4. Column web buckling and beam flange buckling under compression are not considered in such modeling procedure.

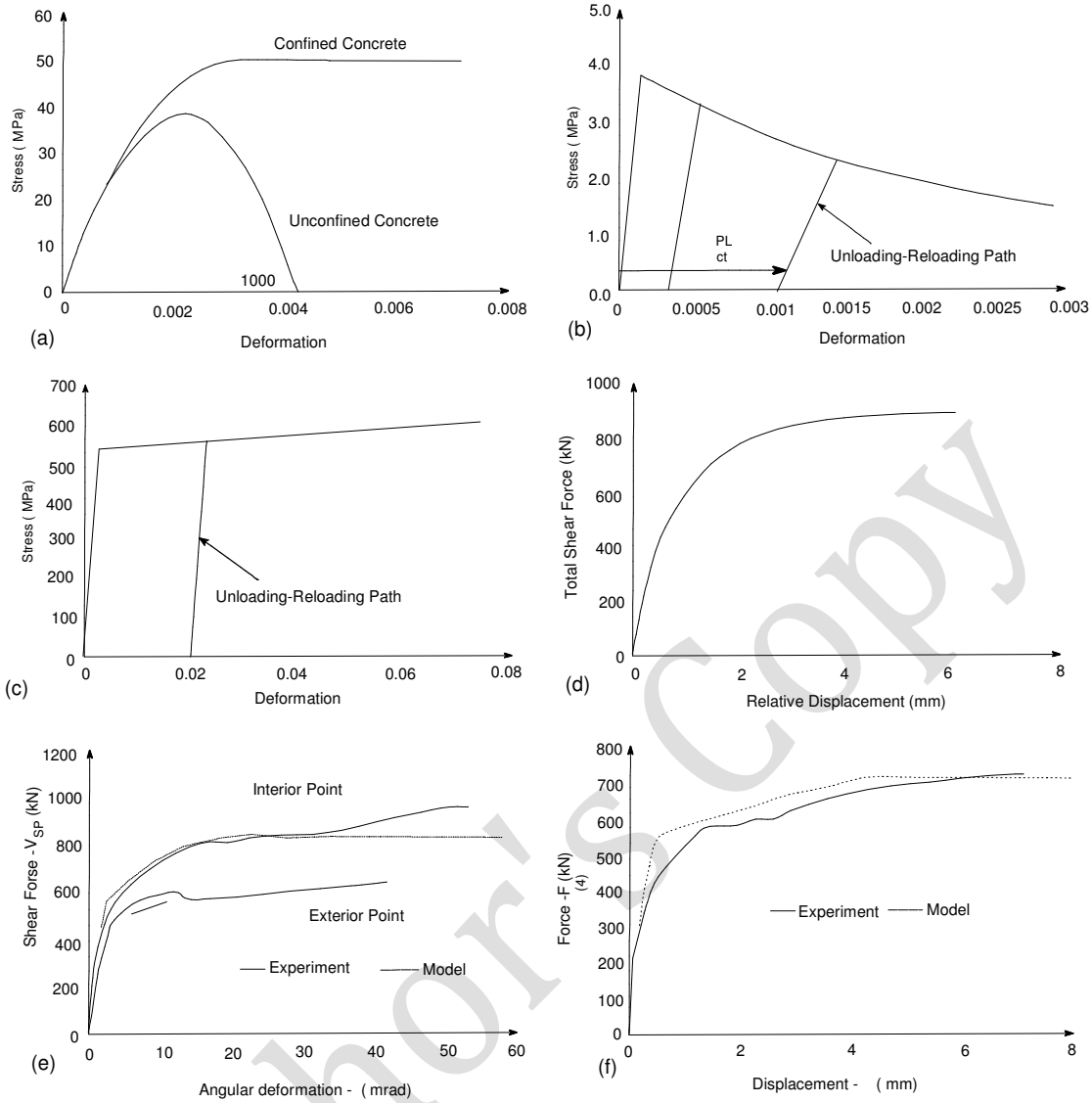

Fig. 15: Component constitutive relationships: a) concrete in compression; b) concrete in tension; c) reinforcing steel; d) shear stud; e) panel zone in shear; and f) lower T-Stub in tension

Fabbrocino et al. 2002:

1. Modeling the cross section of composite beams is achieved through a modification of the well known Newmark's kinematic model, as shown in **Figure 16**.

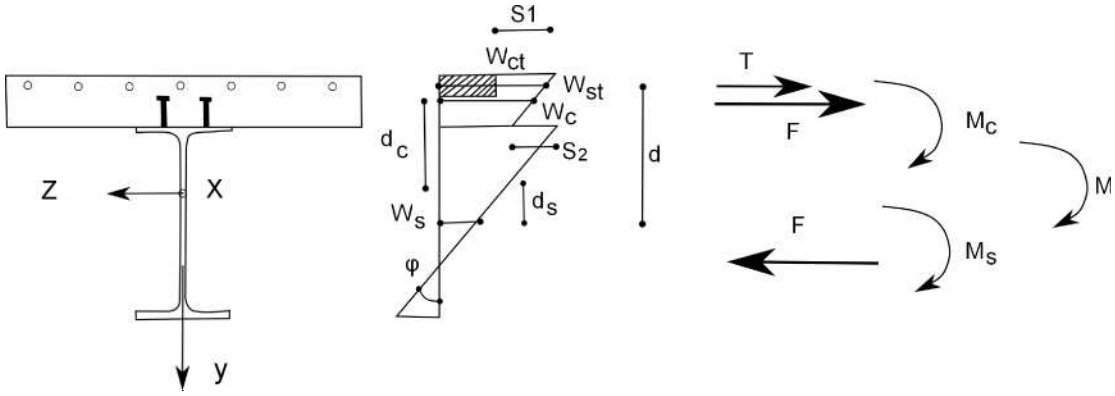

Fig. 16: Cross-section model under negative bending

This approach requires the definition of the slab effective width depending on the type of loading (hogging or sagging), and on the connection detailing at the beam end. A linear strain pattern is then applied to each component of the cross-section. Under the assumption that the curvature and the rotation for each of the components is the same (eg. for both the concrete slab and the steel profile) the uplift is neglected. Using analytical procedures, the tensile stresses developed in the concrete slab, the slip between the different components of the cross section, the interaction force, F, the global bending moments in the steel profile, M_s, and the concrete slab, M_c, as well as the moment-curvature relationship of the cross-section can be obtained.

2. Modeling the continuous composite beam is based on a combination of the main behavioral aspects on the different regions of the beam (i.e. Newmark's model is used for sagging moments, whereas its modified version is used when cracked zones of the beam are considered). The moment-curvature relationship in each section of the beam can be then defined through an iterative process. Once the generalized moment-curvature relationship is established, rotations and displacements can be obtained by integration of the curvature distribution. The numerical procedure for the solution of a simple structural system of a beam characterized by geometrical and mechanical symmetry is based on the compatibility method, therefore, the support bending moment is the main unknown and the beam is statically determined. The reader is referred to Fabbrocino et al. 2002 for a step-by-step guidance for the solution of the composite section and beam.

4. MODELING OF THE PANEL ZONE IN SEMI-RIGID STEEL CONCRETE COMPOSITE CONNECTIONS

When moment resisting frames are subjected to horizontal loading such as earthquake excitation, unbalanced moments occur at the beam-to-column connections resulting to shear deformations in the panel zones of the columns. Therefore, the behavior of the panel zone plays a significant role in determining the overall stiffness and capacity of the frame. In addition to this, in terms of seismic design, the panel zone can have a significant influence on the distribution of plasticity and energy dissipation mechanisms, and in turn significant effects on the overall performance of the structure.

This section deals with the modeling of the panel zone region within the beam-to-column joints of SCC moment resisting frames. This particular model proposed by Castro et al. (2004) is based on a realistic stress distribution at the edges of the panel, aiming to account for the location of the neutral axis. This methodology enables assessment of the shear stress distribution through the panel depth representing the distribution of the plasticity in the vicinity of that region. Both shear and bending deformations are considered in the elastic and post-elastic stages. The additional resistance of the panel zone owing to the contribution of the column flanges is also taken into account by considering the column depth and flange thickness.

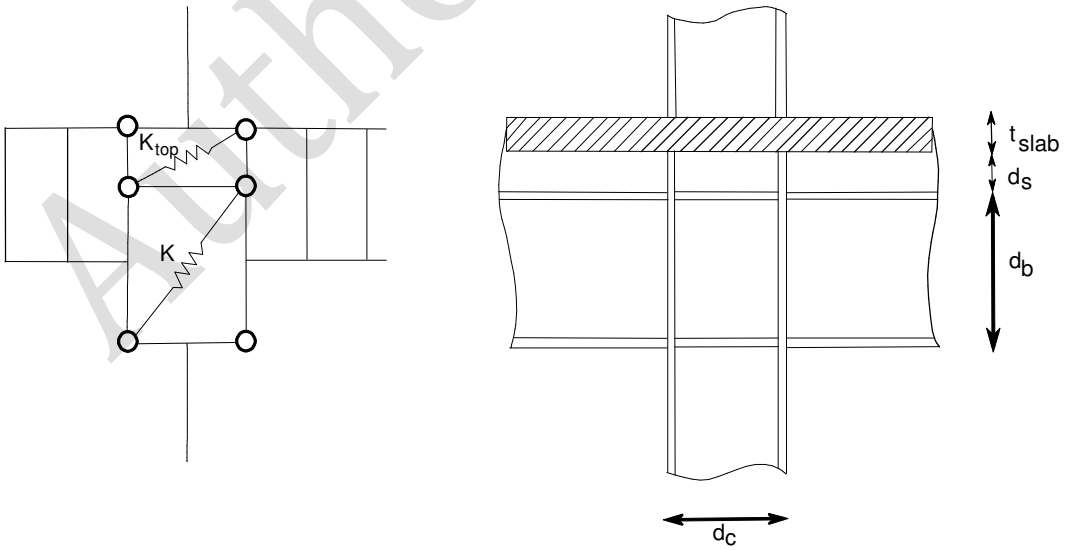

Fig. 17: Numerical and analytical representation of joint models

4.1 Procedures and details

With reference to **Figure 16**, the physical dimensions of the panel zone, d_c and d_b, are taken into account. The part of the column being in contact with the slab is modeled through an assemblage of links on top of the panel. This modeling approach is essentially a determination of the spring properties of both the 'panel zone' and the 'top panel' which are derived analytically allowing for implementation in frame analysis software. The procedure establishes an analogy between the analytical (consisting of the actual connection) and the corresponding numerical model for frame analysis, as shown in **Figure 18**.

The location of neutral axis is calculated considering a linear stress distribution, based on the assumption that the SCC beam behaves elastically until the panel yields.

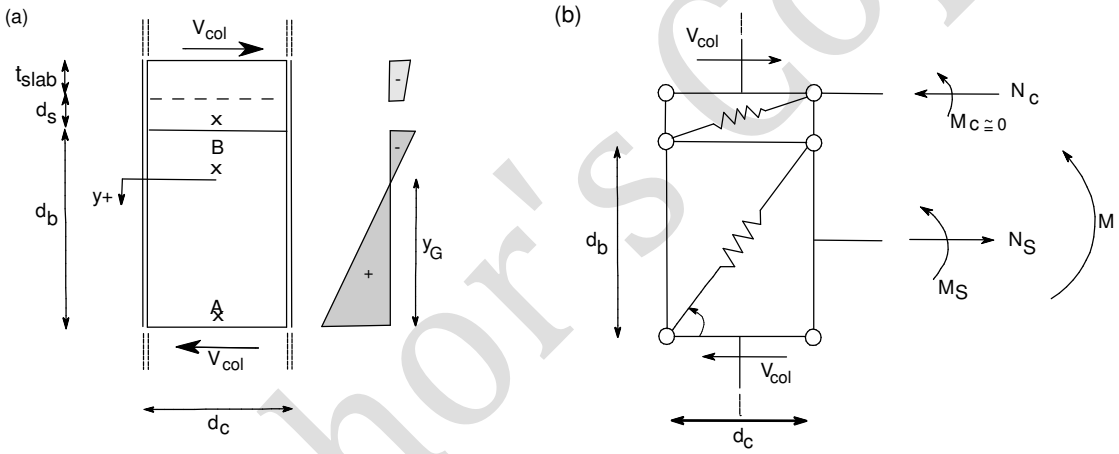

Fig. 18: Analytical and numerical representation of joint models

An assessment of the effective width of the slab in the vicinity of the connection is also required. For positive moment (sagging moments), it is assumed that the slab is limited to the contact width of the column flange width, b_c. For negative moment (hogging moments), the slab is not considered, under the assumption that the reinforcement is not anchored to the column.

4.1.1 Notion of calculations

The main aspect of the proposed model is the determination of the spring properties for both the panel zone and the top panel. For a given moment carried by the SCC beam, a corresponding equivalent shear is applied to the panel in the numerical model. The stiffness that should be used in the numerical model can be then

determined from the distortion caused to the analytical model owing to the application of moment. Furthermore, the difference between load level corresponding to first and full yielding of the panel can be derived given that the shear stress distribution through the panel is known. The procedure needed to be followed by the engineer for derivation of these important parameters for both elastic and post elastic ranges is outlined below.

This section serves as a numerical guideline; the reader is referred to J.M Castro et al. 2005 to exploit the complete set of equations.

Elastic range:

1. The neutral axis location of the steel beam and in turn its second moment of area can be calculated under the assumption that the steel beam behaves in an elastic manner up to yielding of the panel zone.
2. The ratio of axial force (Ns) and bending moment (Ms) carried by the beam can be then obtained using analytical procedures.
3. The total moment (M) acting to the connection can be then calculated in the numerical model using Equation (29). The moment (Mc) developed in the slab, is considered to have insignificant influence and therefore it is ignored.

$$M = Ms + Ns\left[\frac{d_b}{2} + d_s + \frac{t_{slab}}{2}\right] \quad (29)$$

4. The equivalent moment carried by the panel can be then obtained from Equation (30).

$$V_{eq} = \frac{Ms}{d_b} + \frac{Ns}{2} - V_{col} \quad (30)$$

Where: $V_{col} = \frac{M}{h_s}$ and h_s is the storey height

5. From the analytical model, knowing the normal stress distribution of the composite section, the shear force and bending moment distributions can be obtained.
6. Using the principle of virtual work (**Figure 19**) and the calculated shear force and bending moment distributions, the relative horizontal displacement can be obtained. Having the application of opposite unit forces in the virtual system, the internal virtual forces (V_{int}, M_{int}) can also be obtained.

7. Using the calculated equivalent shear force (V_{eq}) and the relative horizontal displacements, ($|\Delta_{shear}|, |\Delta_{bending}|$), the elastic stiffness to be used in the numerical model is calculated by:

$$K_{el} = \frac{V_{eq}}{|\Delta_{shear}|+|\Delta_{bending}|} \quad (31)$$

8. Using the calculated elastic stiffness, the relative drift of the panel ($\Delta_{y,el}$) at the onset of yielding can be obtained analytically.
9. Finally, using the calculated elastic stiffness and the relative drift of the panel zone, the elastic stiffness and the relative drift of the spring can be obtained using the Equation (32) and (33).

$$K_{el,spring} = \frac{K_{el}}{\cos^2 a} \quad (32)$$

$$\Delta_{el-y,spring} = \frac{\Delta_{y,el}}{\cos a} \quad (33)$$

Where: a is the angle of the spring as indicated in **Figure 18**.

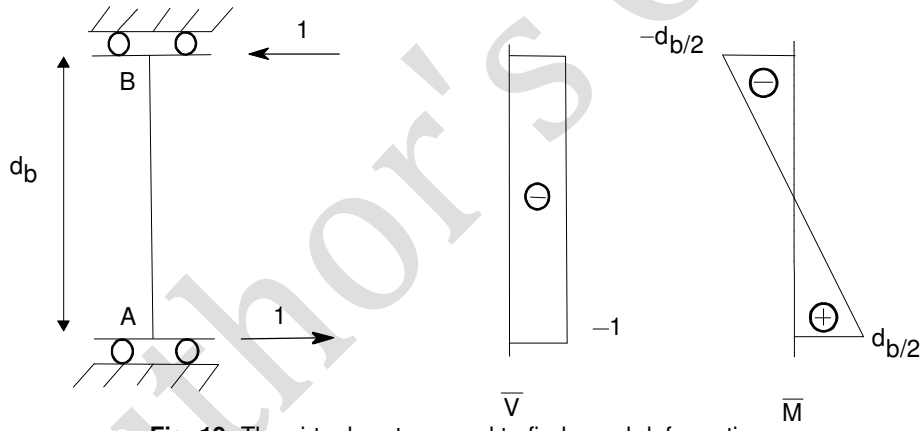

Fig. 19: The virtual system used to find panel deformations

Post elastic range:

1. Beyond the yielding of the panel, the shear stiffness of the column web is assumed to drop to the strain hardening stiffness of the material. Consequently, the post-elastic stiffness of the panel is provided by the strain hardening of the column web by the flanges and a portion of the column web delimiting the panel zone, as shown in **Figure 20**. Following the same assumption for the beam remaining largely elastic, and by following similar procedures to those described for the elastic range, the post elastic stiffness for the panel can be obtained from Equation (34).

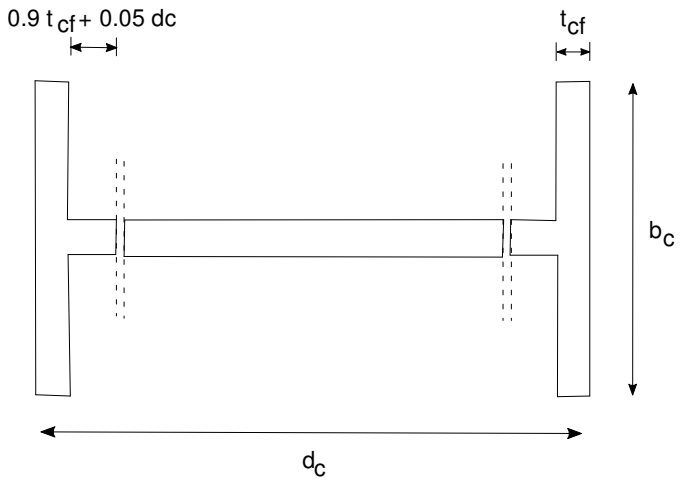

Fig. 20: The cross-section definition for the post-elastic range

$$K_{pl} = \left[\mu \frac{V_{eq}}{\Delta_{shear}}\right] + \left[\frac{V_{eq}}{\Delta_{bending}} \frac{2I_t}{I_{col}}\right] \quad (34)$$

Where:

μ = strain hardening parameter

I_t = second moment of area of the T-section obtained analytically

I_{col} = second moment of area of the column obtained analytically

2. The relative deformation, $\Delta_{y,pl}$, of the panel zone in the post-elastic range can be obtained using the principle of virtual work and can be readily derived as:

$$\Delta_{y,pl} = \Delta_{y,el} + \frac{\overline{f_y}\, d_b{}^2}{6E\, d_{CG}} \quad (35)$$

Where:

d_{CG} = distance from the centroid of the T-Section to the external fiber of the column flange

$\overline{f_y}$ = reserve stress in the same fiber after shear yielding of the panel zone

3. Having known the calculated post-elastic stiffness and relative drift of the panel zone, the post-elastic stiffness and relative drift of the spring can be obtained using the Equation (36) and (37).

$$K_{pl,spring} = \frac{K_{pl}}{\cos^2 a} \quad (36)$$

$$\Delta_{\mathrm{pl-y,spring}} = \frac{\Delta_{\mathrm{y,pl}}}{\cos a} \tag{37}$$

4. Finally, the stiffness provided by the panel zone owing to strain hardening in shear (the first term of Equation (34)) is given by:

$$K_{\mathrm{S.Hardening}} = \mu \frac{\mathrm{Veq}}{\Delta_{\mathrm{shear}}} \tag{38}$$

Therefore, the strain hardening stiffness of the diagonal spring can be determined from:

$$K_{\mathrm{S.H-Spring}} = \frac{K_{\mathrm{S.Hardening}}}{\cos^2 a} \tag{39}$$

4.1.2 Moment-rotation relationship of panel zone

The rotational springs in the panel zone are modeled using tri-linear moment-rotation relationships, while using the stiffness derived from the above expressions for the elastic and post-elastic range (later in **Figure 22)**. According to the that figure, the panel zone is expected to behave in an asymmetric manner in tension and compression owing to the presence of concrete slab which influences the stiffness, yield moments, and cyclic behavior of the panel zone. Under negative moment, the concrete slab contribution is ignored owing to cracking of the concrete. Yield points $(M_{py}^{+}, \theta_{py}^{+})$ and $(M_{py}^{-}, \theta_{py}^{-})$ are controlled by the steel yielding and the ultimate points $(M_{pu}^{+}, \theta_{pu}^{+})$ and $(M_{pu}^{-}, \theta_{pu}^{-})$ are controlled by the ultimate strength of the concrete. Under cycling loading, unloading occurs in a straight line with the same slope as the initial stiffness K_e. The reloading is directed towards the previous peak, thereby considering some strength and stiffness degradation.

5. MODELING OF FRAMES USING BEAM ELEMENTS

This section presents an analytical approach for the assessment of SCC frames under earthquake excitation using two-dimensional SCC beam elements (Kim and Engelhardt 2005). In order to model the behavior of SCC beams under earthquake excitation, factors such as the beam-to-column connection details, the local crushing of concrete, the loading pattern on beam as well as the bond behavior between the reinforcing steel and the concrete need to be considered into the modeling. It is widely accepted that three-dimensional FE models can accurately predict the behavior of SCC beams at the expense of time and computational efficiency. On the

other hand, these simpler but reasonably accurate two-dimensional SCC beam models can provide an alternative tool for frame response assessment.

5.1 Beam elements

The beam elements are described as a one-component series hinge-type model combining analytical formulations calibrated against to experimental data and to other data from "sophisticated" described models, while intended to represent the clear span of beams in moment frames (i.e. the length of the beams between column flanges). The two-dimensional SCC beam elements are described by a linear elastic beam with a non-linear zero-length hinge at each end; the resulting element is referred as "complete element". Each of the hinges is described using non-linear rigid-plastic moment-rotation relationships in order to simulate the real structural behavior which was observed from experiments. Each complete element is characterized by 2 external and 2 internal nodes. The internal nodes are located between the connection of the linear elastic beam element and the hinges, while the external nodes connect the entire structure. Each of the external nodes has 3DOFs, 2-translations and 1-rotation in the local coordinate system as presented in **Figure 21**.

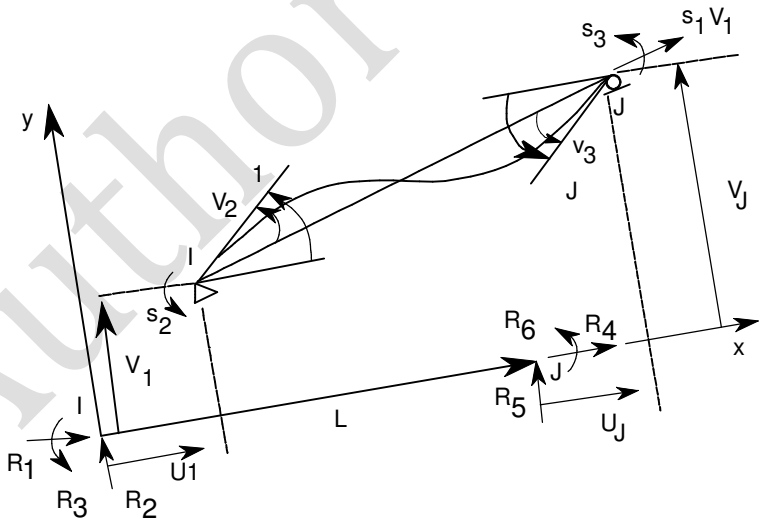

Fig. 21: Element relative forces and deformations in local coordinate system

In the local coordinate system, the element can be considered as a simply supported beam given that the rigid body motions are removed. Based on equilibrium, using the values of relative forces, (s_1, s_2, s_3), all the components of local nodal forces, (R_1 to R_6), can be calculated. The transformation of forces is defined using the following relationship:

$$R = A\,s \tag{40}$$

Where:

A = force transformation matrix (this is well known and can be found in literature, i.e. Przemieniecki 1968)

From the geometry, the transformation from the local displacements, r, to the relative deformations, (v_1, v_2, v_3), is performed by:

$$v = A^{T} r \tag{41}$$

Where:

$$r^{T} = \{U_I, V_I, \theta_I, U_J, V_J, \theta_J\} \tag{42}$$

5.1.1 Element stiffness

The initial stiffness of the aforementioned 'complete element' is that of the linear elastic beam. As gradual yielding occurs at the hinges owing to increased moments at the element ends, the stiffness of the 'complete element' reduces accordingly. In order to obtain the reduced stiffness at any load step after yielding, the instantaneous tangent flexibility of the non-linear rigid-plastic force-deformation relationship for a hinge is combined with the flexibility of the elastic beam element.

A flexibility matrix, f, is first formed for the elastic element including the effects of elastic shear deformation through the following relationship:

$$dq = f\,ds \tag{43}$$

Where:

dq = (dq_1, dq_2, dq_3) = elastic deformation increment at the internal nodes

ds = action increment in which $ds^{T} = \{dF, dM^{I}, dM^{J}\} = \{ds_1, ds_2, ds_3\}$

For hinges at nodes I and J, the incremental action deformation relationship is expressed by:

$$dw_p = \begin{Bmatrix} 0 \\ d\theta_P^I \\ d\theta_P^J \end{Bmatrix} = \begin{Bmatrix} dv_1 - dq_1 \\ dv_2 - dq_2 \\ dv_3 - dq_3 \end{Bmatrix} = f_p\,ds \tag{44}$$

Where:

dw_p= vector of plastic hinge deformations at nodes I and J

$d\theta_P^I, d\theta_P^J$ = incremental plastic rotation at nodes I and J

f_p = hinge or plastic flexibility matrix in which non-zero terms are the second and third elements in the diagonal

Using Equation (43) and (44), the action-deformation relationship can be obtained for the 'complete element' expressed in terms of degrees of freedom, v, as follows:

$$dv = ds + dw_p = F_t ds \tag{45}$$

The hinge flexibility coefficients, f_p, can be simply added to the appropriate coefficients of the elastic element flexibility matrix, f, in order to obtain the tangent flexibility matrix, F_t, for the 'complete element', as shown in Equation (46). Once the 3x3 tangent flexibility matrix is obtained, it is then inverted to obtain the 3x3 tangent stiffness matrix, K_t.

$$F_t = \begin{vmatrix} \frac{L}{EA} & 0 & 0 \\ 0 & \frac{L}{EA^+}F_{ii} + \frac{1}{GA_sL} + f_p^i & -\frac{L}{EA^+}F_{ij} + \frac{1}{GA_sL} \\ 0 & -\frac{L}{EA^+}F_{ij} + \frac{1}{GA_sL} & \frac{L}{EA^+}F_{jj} + \frac{1}{GA_sL} + f_p^j \end{vmatrix} \tag{46}$$

Where:

EA^+ = flexural rigidity of the composite beam

EA = axial rigidity of the composite beam

GA_s = effective shear rigidity of the composite beam

F_{ii} = F_{ij} = 1/3 and F_{jj}= 1/6 for a uniform member

f_p^i, f_p^j = flexibility of hinges at nodes I and J

5.1.2 Hysteretic rules

Due to the cross-sectional asymmetry of the SCC beam, the response will be different for positive and negative moments. As a result, a hinge must discern the load paths to model the hysteretic behavior of SCC beam for an arbitrary cyclic loading. Apart of the cross-sectional asymmetry, the hysteretic rules employed for the complete element need to take into account factors such as the strength deterioration and the stiffness degradation.

In this part of the chapter, the hysteretic rules are determined from the modification of Lee's model (1987) in order to better fit the curves and the non-linear behavior of experimental test specimens. This model employs a specified multi-linear moment-rotation relationship based on two bi-linear curves.

For the monotonic loading, two bi-linear moment-rotation relationships are employed to consider the asymmetrical cross-section and the early cracking of the concrete slab under negative moments (**Figure 22a**). For the cyclic loading, the moment-rotation relationships of the steel beam are modified in order to account for the effect of the concrete slab (i.e. crack closing and opening) (**Figure 22b**).

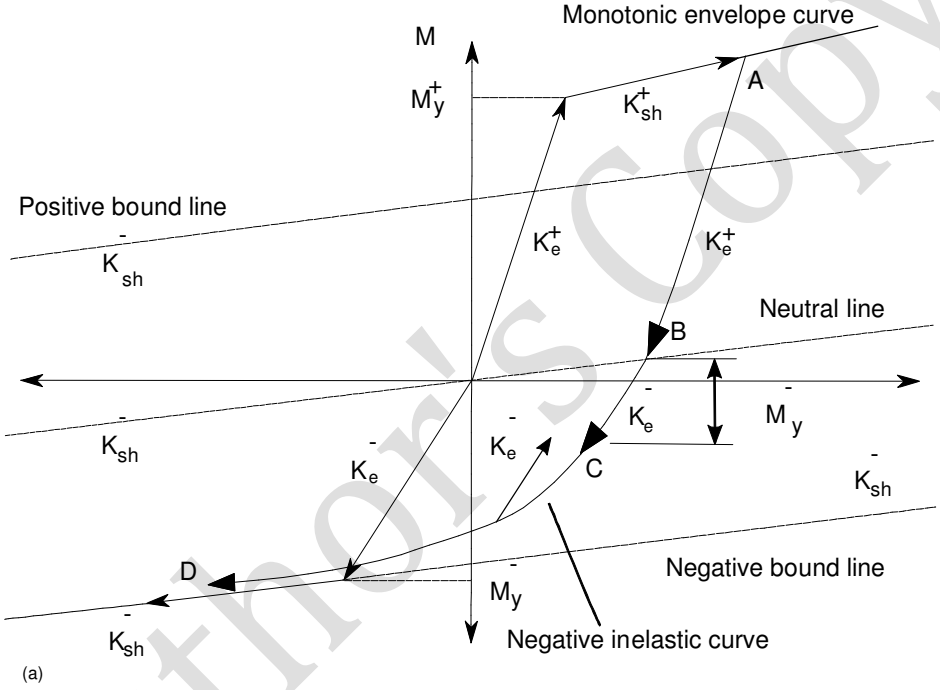

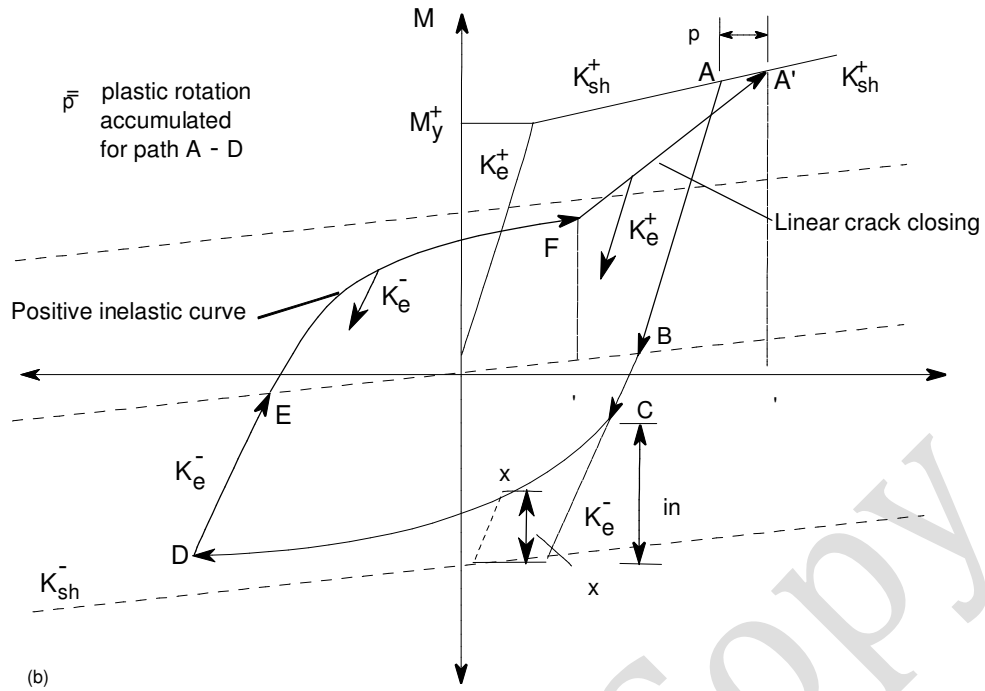

Fig. 22: Proposed cyclic moment-rotation model of a SCC beam; a) monotonic model and stiffness degradation for negative moment; b) stiffness degradation and pinching for positive moment

The basic parameters describing the moment-rotation relation is the moment at the yielding point, and the elastic and inelastic stiffness for both positive and negative bending moments. These parameters can be readily obtained analytically. The value of the strain hardening stiffness is expressed as a fraction of the respective elastic stiffness which is following (i.e. the 2.5% of elastic stiffness in the positive bending and 5% of elastic stiffness in the negative bending).

The engineer is then required to calculate the effective width of the concrete slab on each side of the beam centerline for computing the positive elastic stiffness. This will enable the calculation of the second moment of inertia of the transformed SCC section. The effects of slip between the concrete and the steel on the positive elastic stiffness are taken into account through the use of a fraction of the second moment of inertia of the transformed SCC section. The calculation of the moment of inertia for the negative elastic stiffness needs to be performed, taking into account the steel beam section and the reinforcing steel bars within the effective slab width. The varying moment of inertia of SCC and cracked sections along the length of the beam is assumed to be equivalent to a uniform moment of inertia of a cracked section with reinforcing bars within the effective width.

5.1.2.1 Calculation of moment at the yielding and ultimate point

Using a plastic stress distribution for SCC beams (**Figure 23**), the ultimate moment (Mmax) at the connection can be obtained. The positive yield moment (My^+) is assumed to be a fraction of the calculated ultimate moment. The negative yield moment (My^-) is the plastic moment of both the steel beam section and the reinforcing steel bars within the effective width.

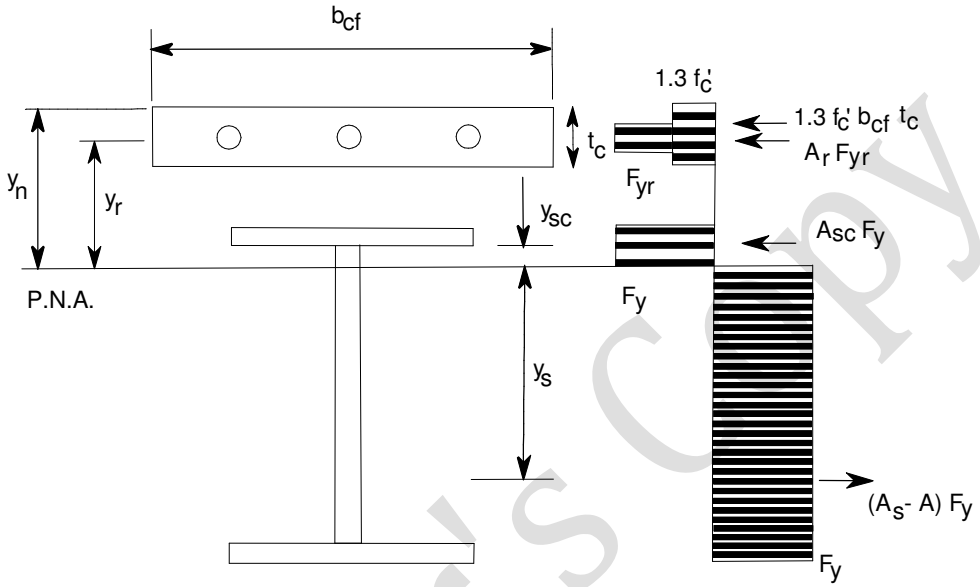

Fig. 23: Plastic stress distribution for composite beam

The contribution of the concrete slab to the ultimate moment at the connection is determined using the column width and a concrete compressive bearing stress of 1.3f'c, due to concrete confinement near the face of the column.

6. Modelling of SCC frames with concrete-filled steel columns

The advantages of concrete-filled steel (CFS) structures in terms of high strength, high ductility and large energy absorption led to their extensive use in high-rise structures in earthquake prone regions.

This section presents a numerical procedure for the non-linear inelastic analysis of CFS frames based on a fiber beam-to-column element. The non-linear response of SCC frames is captured through the inelasticity of materials or due to changes in the frame geometry. Global geometric nonlinearities (P-δ effects) are taken into account by the use of stability functions derived from the exact stability solution of a beam-to-column element subjected to axial forces and bending moments. The spread of

plasticity over the cross-section and along the member length is captured by tracing the uni-axial stress-strain relationships of each fiber on the cross sections located at the selected integration points along the member length. The non-linear equilibrium equations can be then solved using an incremental iterative scheme, based on the generalized displacement control method.

6.1 Fiber beam-to-column element and material nonlinearity

The gradual plastification of a composite cross-section can be described using the concept of fiber section model, similarly to the modeling of the concrete slabs in **Section 1**. The fiber model is presented in **Figure 24**. The concept behind this model is rather simple; the cross-sectional area of the SCC element is subdivided into fibers represented by their area, A_i, and coordinate location (y_i, z_i - with origin the centroid of the section). Different material properties (eg. concrete confined and unconfined, steel, reinforced steel) can be assigned to each of the fibers. Based on the relevant constitutive material models, the fiber strains are used to calculate the fiber stresses, which are in turn integrated over the cross sectional area to obtain stress resultants (i.e. forces and moments).

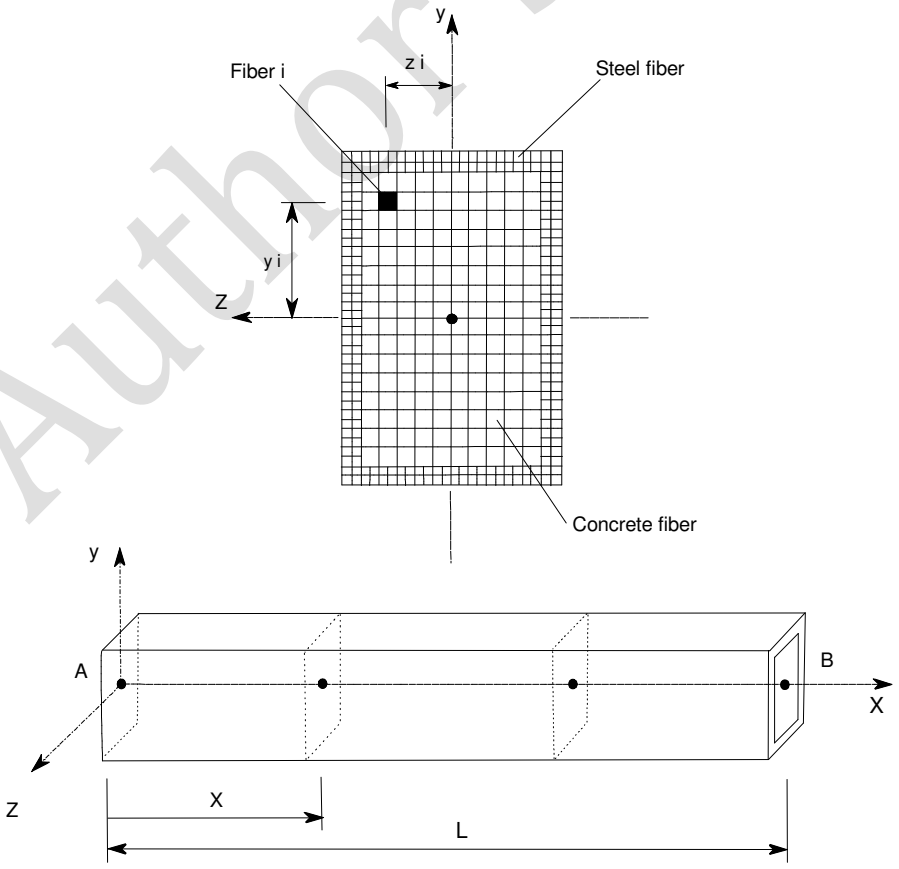

Fig. 24: Fiber hinge concept

Using the fiber model, a number of assumptions have been made as follows:

1. Sections remain plane after bending
2. Due to the latter assumption, the cracking is considered to be smeared and normal to the member axis
3. Torsional and shear effects are ignored
4. Multi-axial stress states (due to the confinement effects) can be included in the model by increasing the concrete strength and modifying its post-peak response
5. Local buckling effects or initial stress arising from thermal effects or erection loads are typically not included

6.2 Confinement of concrete-encased steel sections

In order to utilize the material constitutive models described in the previous sections, the concrete confinement zones need to be identified (**Figure 25**). Several methods for the identification of the confined zones have been suggested for partially- and fully-encased sections and confinement factors, k, have been developed for use in numerical modeling. According to EC8 the confinement factor, k, is given by:

$$k = 1.0 + 5.0\,\alpha_c\,f_1/f_{co} \qquad \text{for} \quad f_1/f_{co} < 0.05 \tag{47}$$

$$k = 1.125 + 2.5\,\alpha_c\,f_1/f_{co} \qquad \text{for} \quad f_1/f_{co} \geq 0.05 \tag{48}$$

Where:

α_c = confinement effectiveness coefficient (Area of concrete / Area of confined concrete)

f_1 = lateral confinement pressure from transverse reinforcement

f_{co} = unconfined concrete compressive strength

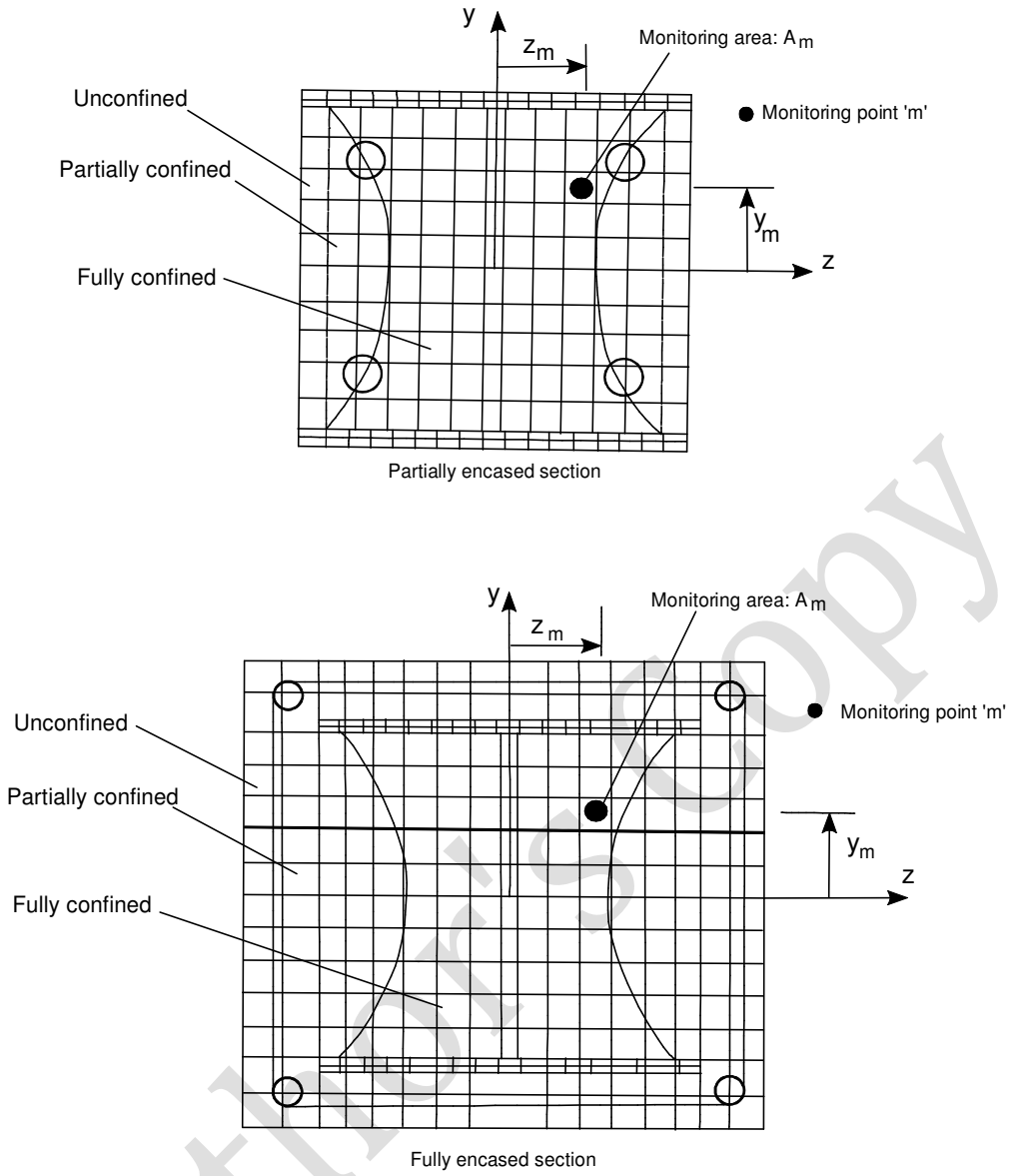

Fig. 25: Confinement zones and distribution of monitoring points of SCC sections

6.3 Local flange buckling

The flange buckling is a phenomenon that largely depends on the width-to-thickness ratio, the boundary (i.e. restraint) conditions and the material properties of the components comprising the section. The effect of the local flange buckling is the reduction of the ultimate strength of the section, and/or the diminishing of its rotational capacity in the inelastic range. Additionally, the ductility of encased SCC members is adversely affected by local buckling and this needs to be considered when estimating the rotational capacity.

To account for the local buckling of bare and encased steel sections, simple methods have been developed and can be readily utilized in a frame analysis software. One of

the most popular methods has been developed by Ballio et al 1987. In this approach, the cross-section is divided into a finite number, i, of strips with each strip having an assigned area. If the compressive strain in any strip exceeds the critical strain, ε_{cr}, the area of the strip reduces to zero for the subsequent load cases. In order to extend the applicability of this method beyond the elastic limit into the inelastic range, the elastic critical stress is divided by the yield strain, as it is represented in the following relationship:

$$\frac{\varepsilon_{cr}}{\varepsilon_y} = \frac{k\,\pi^2\,E}{12\,\sigma_y(1-\nu^2)\left(\frac{\chi_i}{t}\right)^2} \tag{49}$$

Where:

χ_i = distance between the centroid of the strip and the plate connection

t = thickness of the plate

k = confinement factor

E = Modulus of elasticity of steel

v = Poisson's ratio

6.4 Geometric non-linear P-δ effect

Geometric nonlinearities can be classified in two categories. The first category is related to the global geometric nonlinearities, usually referred to as P-δ effects. The second category is related to local geometric nonlinearities (i.e. local buckling), which are generally neglected in frame analysis (while they are carefully considered in advanced finite element analyses with discretized models). The global geometric nonlinearities can be incorporated in the models following basic procedures used in non-linear frame analysis. One of these procedures employs the updated Langarian formulation in order to account for geometric nonlinearities such as large displacements and rotations.

In most of the analyses of multi-storey structures subjected to earthquake excitation, the effects of the combination of gravitational forces and lateral displacement are ignored. The effects are often referred as second order effects. The reason behind overlooking the second order effects can be explained by the fact that traditionally, in low rising reinforced concrete structures (i.e. structures with low natural period and small lateral displacement response) subjected to earthquake excitation, the second

order effects are insignificant and therefore neglected. As steel structures become taller nowadays, the P-Delta effects are amplified due to the corresponding increase of lateral displacement.

The effect of axial force acting through the relative transverse displacement of the member ends known, as P-δ effect, can be taken into account in the modeling by using the geometric stiffness matrix, $[K_g]$, as:

$$[K_g] = \begin{bmatrix} [K_s] & -[K_s]^T \\ -[K_s]^T & [K_s] \end{bmatrix} \tag{50}$$

Where:

$$[K_s] = \begin{bmatrix} 0 & \alpha & -b & 0 & 0 & 0 \\ \alpha & c & 0 & 0 & 0 & 0 \\ -b & 0 & 0 & 0 & 0 & 0 \\ 0 & 0 & 0 & 0 & 0 & 0 \\ 0 & 0 & 0 & 0 & 0 & 0 \\ 0 & 0 & 0 & 0 & 0 & 0 \end{bmatrix} \tag{51}$$

and

$$\alpha = \frac{M_{zA} + M_{zB}}{L^2} \quad b = \frac{M_{yA} + M_{yB}}{L^2} \quad c = \frac{P}{L} \tag{52}$$

M_{zA}, M_{zB}, M_{yA}, M_{yB} = end moments with respect to z and y axes respectively

P = axial force

L = length of the element

The tangent stiffness matrix of a beam-column element is then obtained by the follow relationship:

$$[K]_{12 \times 12} = [T]^T_{6 \times 12} \times [K_e]_{6 \times 6} [T]_{6 \times 12} + [K_g]_{12 \times 12} \tag{53}$$

Where:

$$[T]_{6 \times 12} = \begin{bmatrix} -1 & 0 & 0 & 0 & 0 & 0 & 1 & 0 & 0 & 0 & 0 & 0 \\ 0 & 0 & -1/L & 0 & 1 & 0 & 0 & 0 & 1/L & 0 & 0 & 0 \\ -b & 0 & 0 & 0 & 0 & 0 & 0 & 0 & 1/L & 0 & 1 & 0 \\ 0 & 0 & 0 & 0 & 0 & 0 & 0 & -1/L & 0 & 0 & 0 & 0 \\ 0 & 0 & 0 & 0 & 0 & 0 & 0 & -1/L & 0 & 0 & 0 & 1 \\ 0 & 0 & 0 & 0 & 0 & 0 & 0 & 0 & 0 & -1 & 0 & 0 \end{bmatrix} \tag{54}$$

and

$[K_e]_{6 \times 6}$ = element stiffness matrix given by $\{\Delta F\} = [K_e]\{\Delta d\}$

The reader is referred to Thai & Kim 2011 for details on how to derive the element stiffness matrix.

6.5 Constitutive models

Any of the constitutive models presented in the previous sections for steel, concrete and steel reinforcement can be applied for modeling the material characteristics of the concrete encased steel sections of the SCC frames.

7. SUMMARY

The validity of the above case studies has been verified by comparing the numerical predictions with experimental data obtained from a wide range of structural systems subjected to static and hysteretic loadings. Full details of these comparative studies are presented in the literature. However, such laws and models are usually dependent on parameters which are evaluated through the particular use of the experimental data and it is in the designers' discretion to chose and interprets these when data used for specific purposes. In this chapter, it has been attempted to generalize the constitutive models for a number of applications. On the other hand, the lack of generality and objectivity that characterizes most FE packages can only be balanced through the use of material models which are compatible with valid experimental information. In fact, the work presented in this chapter is considered as a step towards these directions.

The modeling of SCC members in this chapter serves primarily (i) the computation of the response of such members when they are subjected to seismic actions and (ii) acts as a vehicle for carrying out the state determination of the section (or integration point) to a frame element and ultimately to the whole frame assembly. The outcome of the former application is typically the moment-curvature response under a constant axial load. The latter application typically returns section forces that correspond to given section deformations (in uni-axial bending, axial strain and curvature).

In earthquake engineering, the stiffness of the column members is one of the most important parameters of the entire structural systems since it governs the lateral resistance of the frame. The natural period of vibration of the frame decreases with increasing stiffness but also increases with increasing mass. Therefore, the members comprising the frame need to be accurately simulated in order to derive the stiffness and mass matrices to be accounted for the frame analysis. According to the typical response spectra, the acceleration response of a SCC frame reduces with increased natural period. This implies that a composite structure will have to resist lower base shear, therefore, the earthquake effects will be less significant. The displacement response of the structure also increases proportionally with increasing natural period. For the case of increased lateral displacements, second order effects (P-δ effects) could be developed which will determine the design and amplify the demand on the structure. The engineer is required to reduce the influence of the second order effects by controlling the lateral displacement of the frame providing ductility in the beams, columns and connections. As a result, the accurate analysis of each individual component plays important role in the aseismic design. In the holistic frame assembly, global geometric nonlinearities can be incorporated in the models following basic procedures used in the non-linear frame analysis (i.e. modification of the stiffness matrix).

Using non-linear static analysis, the engineer can obtain information on the global ductility and strength of the structure through force-displacement relations. At each point on the force-displacement curve, the engineer can check the member behavior and see whether the limit states are fulfilled. Weak areas and progressive hinge formation on the structural frame are revealed during the analysis.

8. REFERENCES

Aribert, J-M., & Lachal, A. (2000). Cyclic behaviour of the shear connection component in composite joints. In Behaviour of Steel Structures in Seismic Area. Proceedings of STESSA 2000 Conference, Montreal, Canada. Balkema: Rotterdam, 105-112.

Balan, T.A., Filippou, F.C., & Popov, E.P. (1997). Constitutive model for 3D cyclic analysis of concrete structures. Journal of Engineering Mechanics, 123(2), 143-153.

Ballio, G., Calado, L., Iori, I., & Mirabella Roberti, G. (1987). I problemi delle grandi costruzioni in zona sismica. Associazione Italiana Cemento Armato e Precompresso, Roma, 31-44.

Braconi, A., Salvatore, W., Tremblay, R., & Bursi O.S. (2007). Behaviour and modeling of partial-strength beam-to-column composite joints for seismic applications. Earthquake engineering and structural dynamics, 36, 142-161.

Castro, J.M., Elghazouli, A.Y., & Izzuddin, B.A. (2005). Modelling of the panel zone in steel and composite moment frames. Engineering Structures, 27(1), 129-144.

Cotsovos, D.M., & Kotsovos, M.D. (2011). Constitutive modelling of concrete behaviour, 147-175. In Papadrakakis, M., Fragiadakis, M., & Lagaros , N. D. (Eds.), Computational Methods in Earthquake Engineering. Computational Methods in Applied Sciences, Springer Netherlands.

Fabbrocino, G., Manfredi, G., & Cosenza, E. (2002). Modelling of continuous steel-concrete composite beams: computational aspects. Computers & Structures, 80(27-30), 2241-2251.

Kim, D.K., & Engelhardt, M.D. (2005). Composite beam element for nonlinear seismic analysis of steel frames, Journal of structural engineering, 131, 715-724.

Krawinkler, H. (1978). Shear in beam-column joints in seismic design of steel frames. Engineering Journal, 15(3), 82-91.

Menegotto, M. & Pinto, P.E. (1973). Method of Analysis for Cyclically Loaded R.C. Plane Elements Including Changes in Geometry and Non-Elastic Behaviour of Elements under Combined Normal Force and Bending, IABSE, Report of the Working Commissions, Band 13, Symposium on Resistance and Ultimate Deformability of Structures Acted on by Well Defined Repeated Loads, Lisboa.

Newmark, N.M., Siess, C.P., & Viest, I.M. (1951). Tests and Analyses of Composite Beams with Incomplete Interaction. Proceedings, Society for Experimental Stress Analysis, Vol. 9, No. 1, 75-92.

Ollgaard, J.G., Slutter, R.G., & Fisher, J.W. (1971). Shear strength of stud connectors in lightweight and normal-weight concrete. AISC Engineering Journal, 8(2), 55-64.

Park, R., & Paulay T. (1975). Reinforced Concrete Structures. NewYork: J.Wiley and Sons.

Piluso, V., Faella, C., & Rizzano G. (2001). Ultimate behavior of bolted T-stubs. I: theoretical model. Journal of Structural Engineering, 127(6), 686-693.

Przemieniecki, J.S. (1968). Theory of Matrix Structural Analysis, McGraw-Hill Companies.

Stevens, N.J., Uzumeri, S.M., Collins, M.P., & Will, G.T. (1991). Constitutive model for reinforced concrete finite element analysis. ACI Structural Journal, 88(1), 49–59.

Thai, H.T., & Kim, S.E. (2011). Nonlinear inelastic analysis of concrete-filled steel tubular frames. Journal of constructional steel research, 1797-1805.

Uchida, N., & Tohki, H. (1997). Design of high-rise Building using Round Tubular Steel Composite Columns. IABSE International Conference on Composite Construction Conventional and Innovative, Innsbruck, 16-18 September.

Zhao, H., Yuan, Y., & Ye, Y. (2012). Simplified nonlinear simulation of steel-concrete composite beams. Journal of Constructional Steel Research, 71, 83-91.

Zona, A., Barbato, M., & Conte, J.P. (2008). Nonlinear seismic response analysis of steel-concrete composite frames. ASCE Journal of structural engineering, 123:6(986).